

**CFD STUDY ON THE CORRELATION FOR A PARTIALLY
SUBMERGED ORIFICE FLOW**

DERIC LEE KAR WAI

**A project report submitted in partial fulfilment of the
requirements for the award of Bachelor of Engineering
(Honours) Chemical Engineering**

**Lee Kong Chian Faculty of Engineering and Science
Universiti Tunku Abdul Rahman**

May 2021

DECLARATION

I hereby declare that this project report is based on my original work except for citations and quotations which have been duly acknowledged. I also declare that it has not been previously and concurrently submitted for any other degree or award at UTAR or other institutions.

Signature : *Deric*

Name : Deric Lee Kar Wai


ID No. : 17UEB01206

Date : 16th April 2021

APPROVAL FOR SUBMISSION

I certify that this project report entitled “**CFD STUDY ON THE CORRELATION FOR A PARTIALLY SUBMERGED ORIFICE FLOW**” was prepared by **DERIC LEE KAR WAI** has met the required standard for submission in partial fulfilment of the requirements for the award of Bachelor of Engineering (Honours) Chemical Engineering at Universiti Tunku Abdul Rahman.

Approved by,

Signature : 

Supervisor : Ir. Dr. Teoh Hui Chieh

Date : 16th April 2021

The copyright of this report belongs to the author under the terms of the copyright Act 1987 as qualified by Intellectual Property Policy of Universiti Tunku Abdul Rahman. Due acknowledgement shall always be made of the use of any material contained in, or derived from, this report.

© 2021, Deric Lee Kar Wai. All right reserved.

ACKNOWLEDGEMENTS

I would like to express my gratitude to everyone that enabled me to complete this project. I would like to convey my sincere gratitude to my research supervisor, Ir. Dr. Teoh Hui Chieh and industrial supervisor, Ir. Dr. Yeoh Hak Koon for their invaluable advice, guidance and patience in shaping and completing this research topic.

CFD STUDY ON THE CORRELATION FOR A PARTIALLY SUBMERGED ORIFICE FLOW

ABSTRACT

The purpose of this study is to develop a CFD model that allows the correlation study for a partially submerged circular orifice flow in open channel. Three phenomena driven by gravity were included in this study, which are free discharge orifice (**Case A**), partially submerged orifice flow in downstream (**Case B**), and partially submerged orifice flow in both stream (**Case C**). Validation of model was carried out using **Case A**, yielding 0.35–38.05% deviation against the models from literature. The relationship between the volumetric flow rate with the orifice diameter and water level difference was analysed and the hypothesis that volumetric flow rate increases as the water level difference and orifice diameter increase in partial submerged condition was proven for **Case B** and **C**. Furthermore, the effect of orifice diameter to the volumetric flow rate was found out to be greater than that of the water level difference. Lastly, correlation of volumetric flow rate with water level difference and orifice diameter for **Case B** and **C** were determined through the model developed.

TABLE OF CONTENTS

DECLARATION		ii
APPROVAL FOR SUBMISSION		iii
ACKNOWLEDGEMENTS		v
ABSTRACT		vi
TABLE OF CONTENTS		vii
LIST OF TABLES		ix
LIST OF FIGURES		x
LIST OF SYMBOLS / ABBREVIATIONS		xiii
 CHAPTER		
1	INTRODUCTION	1
1.1	Background	1
1.2	Importance of Study	2
1.3	Problem Statement	3
1.4	Aim and Objectives	4
1.5	Scope and Limitation of Study	4
2	LITERATURE REVIEW	6
2.1	Orifice Flow	6
2.1.1	Free Discharging Orifice Flow	7
2.1.2	Partially Submerged Orifice Flow	14
2.2	CFD Modelling for Orifice and Open Channel Flow	19
2.2.1	Turbulent Overflow on Stepped Spillways	21
2.2.2	Free Flow Past a Sluice Gate	21
2.2.3	Side Weir Flow in Open Channel	22
2.2.4	Free Surface Flow over Triangular Labyrinth Side Weir	22
2.2.5	Free Surface Flow over Side Weir	23
2.2.6	Orifice Flow in a Trough-type Liquid Distributor	24

	2.2.7	Free and Submerged Flow of an Orifice Extended with Circular Pipe	27
	2.2.8	Mutual Effect of Flow in Weir and Gate System	28
	2.2.9	Free Flow through Side Rectangular Orifice	29
	2.3	Summary	32
3		METHODOLOGY	34
	3.1	Introduction	34
	3.2	CFD Theory	34
	3.3	Orifice Geometry and Design	35
	3.3.1	Base Model	35
	3.3.2	3-D Model	37
	3.4	Meshing	37
	3.5	Simulation Setup	39
4		RESULTS AND DISCUSSION	45
	4.1	Mesh Independence Analysis	45
	4.2	Case A – Free Discharge Flow through Orifice	46
	4.2.1	Base Model	46
	4.2.2	3-D Model	48
	4.3	Case B – Partially Submerged at Orifice Outlet	50
	4.4	Case C – Partially Submerged at Both Inlet and Outlet	53
5		CONCLUSION AND RECOMMENDATIONS	57
	5.1	Conclusion	57
	5.2	Recommendations	57
		REFERENCES	58
		APPENDICES	62

LIST OF TABLES

Table 2.1: Average Discharge Coefficients for Free Flow through Circular Orifice (Bos, 1989).	9
Table 2.2: Summary of Discharge Coefficient for Flow under Sluice Gate.	10
Table 2.3: Parameters of Orifice Tested (Brandes and Barlow, 2012).	17
Table 2.4: Guideline for Monitor Residuals (Datawave Marine Solutions, 2019).	21
Table 2.5: Summary of Models for Case A.	32
Table 2.6: Viscous Models for CFD Simulations in Chapter 2.	33
Table 3.1: Parameters for CFD Geometry Model.	35
Table 4.1: Mesh Independence Analysis for Both Models.	45
Table 4.2: Validation of Base Model with Free Discharge Flow through Water Gate.	48
Table 4.3: Validation of Base Model with Weir Flow.	48
Table 4.4: Validation of 3-D model Free Discharge Flow through Circular Orifice.	50

LIST OF FIGURES

Figure 1.1: Example of a Sketch of a Circular Orifice.	2
Figure 1.2: Partially Drowned Orifice (Ahmad, 2012).	2
Figure 1.3: Orifice Flow, (a) Free Discharging, (b) Orifice Outlet is Partially Submerged, (c) Both Sides are Partially Submerged	4
Figure 1.4: Parameters of Interest.	4
Figure 2.1: Free Discharging Orifice (Bos, 1989).	8
Figure 2.2: Flow Past Suice Gate (Bos, 1989).	9
Figure 2.3: Rectangular Side Orifice under Open Channel Flow (Hussain, et al., 2011).	11
Figure 2.4: Variation of Discharge Coefficient for Circular and Rectangular Side Orifices with Different L/B or D/B (Hussain, et al., 2011).	11
Figure 2.5: Steady Free Surface Flow through Circular Orifice (Kubrak, 2015).	13
Figure 2.6: Flow over Sharp-crested Weir (Oshima, et al., 2013)	13
Figure 2.7: Partially Submerged Flow in Circular Orifice (Guo and Stitt, 2017).	14
Figure 2.8: Dimensionless Headwater-to-diameter Relation for a Fully Submerged Circular Orifice Flow and Partially Full Circular Weir Flow (Vatankhah, 2018).	15
Figure 2.9: Schematic of a Partially Submerged Orifice (Brandes and Barlow, 2012).	17
Figure 2.10: Comparison of Model in Steady-state Experiments: Top left (Orifice 1), Top Right (Orifice 2), Bottom (Orifice 3) (Brandes and Barlow, 2012).	18
Figure 2.11: Transient Drainage Experiments with Orifice 1 (Brandes and Barlow, 2012).	19
Figure 2.12: Comparison of Different Turbulence Models with Surface Profiles of Vortex Formation inside Triangle Labyrinth Side Weir (Aydin, 2012).	23

Figure 2.13: Determining the Sensitivity of Results for Different Turbulence Models (Aydin and Emiroglu, 2013).	23
Figure 2.14: Sketch of Orifice Flow in Through-type Liquid Distributor (Yu, et al., 2013).	24
Figure 2.15: Comparison of Observed and Simulated Results (Yu, et al., 2013).	25
Figure 2.16: Velocity Vector Distribution for 0.388 kg/s Inlet (a) and 0.63 kg/s Inlet (b) (Yu, et al., 2013).	26
Figure 2.17: Comparison of Results with Different Distances (Yu, et al., 2013).	27
Figure 2.18: Schematic Diagram for Pipe Overflow Structure (Isenmann, et al., 2016).	28
Figure 2.19: Schematic Diagram of the Combined System from Flow-3D (Sarhan and Jalil, 2018).	29
Figure 2.20: Computational Domain of Side Rectangular Orifice Model (Hussain and Haroon, 2019).	30
Figure 2.21: Tetrahedral Meshing (Hussain and Haroon, 2019).	31
Figure 2.22: Comparison between Results in CFD Model and Experimental Model (Hussain and Haroon, 2019).	31
Figure 3.1: 3-D Sketch of Base Model.	36
Figure 3.2: Translational Symmetry to Convert Base Model into 2-D.	36
Figure 3.3: Dimensions for Base Model.	36
Figure 3.4: Sketch of the 3-D model.	37
Figure 3.5: Finer Mesh Size around Orifice for Base Model.	38
Figure 3.6: Finer Mesh Size around Orifice for 3-D Model.	38
Figure 3.7: Mesh Quality Check Parameters (Ansys, 2015).	38
Figure 3.8: Boundary Conditions for Base Model.	41
Figure 3.9: Boundary Conditions for 3-D model.	42
Figure 3.10: Surface where Volumetric Flow Rate is Measured.	42

Figure 3.11: Free Surface Level and Bottom Level (Ansys, 2013).	42
Figure 3.12: Location for Global Coordinate System.	43
Figure 4.1: Volume Fraction Contour of Free Discharge Flow through Water Gate at Different Water Surface Level. Red Colour Indicates Water and Blue Colour Indicates Air. (a) 290 mm, (b) 270 mm, (c) 250 mm and (d) 230 mm.	47
Figure 4.2: Volume Fraction Contour of Free Discharge Flow through Weir at Different Water Surface Level. Red Colour Indicates Water and Blue Colour Indicates Air. (a) 195 mm and (b) 185 mm.	47
Figure 4.3: Velocity Vectors at the Upstream Domain Case A (Top View).	49
Figure 4.4: Volume Fraction Contour at the Upstream Domain Case A (Top View). Red Colour Indicates Water and Blue Colour Indicates Air.	49
Figure 4.5: Volume Fraction Contour at the Upstream Domain Case B (Side View). Red Colour Indicates Water and Blue Colour Indicates Air.	51
Figure 4.6: Volume Fraction Contour at the Upstream Domain Case B (Top View). Red Colour Indicates Water and Blue Colour Indicates Air.	51
Figure 4.7: Volumetric Flow Rate, Q against Water Level Difference, Δh at different Orifice Diameter, d (Case B).	52
Figure 4.8: Velocity Vectors at the Upstream Domain Case B (Top View).	52
Figure 4.9: Volume Fraction Contour at the Upstream Domain Case C (Side View). Red Colour Indicates Water and Blue Colour Indicates Air.	54
Figure 4.10: Volume Fraction Contour at the Upstream Domain Case C (Top View). Red Colour Indicates Water and Blue Colour Indicates Air.	54
Figure 4.11: Velocity Vectors at the Upstream Domain Case C (Top View).	55
Figure 4.12: Volumetric Flow Rate, Q against Water Level Difference, Δh at different Orifice Diameter, d (Case C).	55

LIST OF SYMBOLS / ABBREVIATIONS

Q	volumetric flow rate, m ³ /h
d	orifice diameter, mm
Δh	water level difference, mm
h_2	water surface level at the downstream domain, mm
C_d	discharge coefficient
g	gravitational acceleration, m/s ²
h	head water above the orifice centre, m
A	orifice cross-sectional area, m ²
L	width of rectangular orifice, m
H_{1r}	water level from the bottom orifice, m
H_{2r}	water level from the top of orifice, m
Y_m	main channel flow depth, m
W	sill height/ weir height, m
B	width of main channel, m
b	width of weir, m
h_{1e}	effective weir head, m
h_1	measured weir head, m
p	weir plate height, m
y	head water above the orifice crest, m
C_w	weir discharge coefficient
C_e	effective discharge coefficient
ω	filling ratio, (h_1/d)
l	orifice thickness, m
H	upstream flow depth, m
k	turbulence kinetic energy, m ² /s ²
ε	kinetic dissipation rate, m ² /s ³
ρ	fluid density, kg/m ³
t	time, s
\vec{v}	fluid velocity vector
p	static pressure, Pa
μ	molecular viscosity, Pa.s
I	unit tensor

S_m	external mass added into the system, kg
CFD	computational fluid dynamics
2-D	two dimensional
3-D	three dimensional
ISO	international organization of standardization
SWMM	storm water management model
VTPSUHM	virginia tech/penn state urban hydrology model
VOF	volume of fluid
RANS	reynolds averaging navier-stokes equations
$k-\varepsilon$	k-epsilon turbulence model
RNG $k-\varepsilon$	renormalised $k-\varepsilon$ turbulence model
FVM	finite volume approach
PISO	pressure implicit with split operator
PRESTO!	pressure staggering option
HPC	high performance computer
$k-\omega$	k-omega turbulence model
SST $k-\omega$	shear stress transport k-omega turbulence model
RSM	reynolds stress model
QUICK	quadratic upstream interpolation for convective kinematics
SIMPLE	semi-implicit method for pressure-linked equations
URF	under relaxation factor

CHAPTER 1

INTRODUCTION

1.1 Background

By definition, orifice refers to a mouthlike aperture, gate or opening (Figure 1.1), commonly located on the surface of water tanks (bottom or side wall) or in a pipe, at which there is a presence of flow. When fluid enters an orifice, the velocity around the orifice increases significantly due to restriction of the cross section, producing a contracted jet from the orifice outlet. Orifice can be used as an artificial restriction integrated in flow system to measure the flow. Other than flow measurement, it can also deliberately increase head loss as well as redirecting or discharge a portion of the main channel flow to alternative channel. In fact, this hydraulic structure was extensively used for flow management purpose, and is implemented in numerous industrial applications, which cover many needs of flow measurement technology (Hussain, et al., 2014). For instance, side orifice that is normally mounted on the vertical surfaces, perpendicularly to the flow direction, was applied in waste water treatment, stormwater management, sedimentation tanks, flocculation and aeration basins. (Hussain, et. al., 2011)

The design of an orifice can be rather simple with just an opening that connects through structures as shown in Figure 1.1. Yet, it is capable to demonstrate its effectiveness in obtaining the desired discharge flow through determining the pressure drop via its shape and geometry. Adam, et al. (2017) state that the orifice geometry determines the pressure drop that was utilised to manage the throttling of a surge tank during renovation or power breakdown, allowing the highest and lowest water level of the surge tank to be determined as well as to control downstream discharge and prevent transient events. That is to say, in determining the accurate pressure drop and desired energy loss through an orifice, optimisation of the orifice geometry can be reasonably useful.

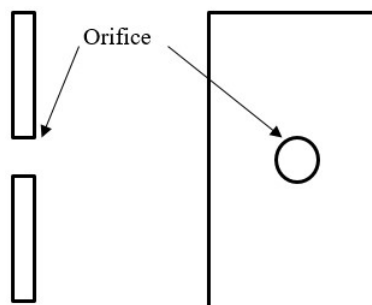


Figure 1.1: Example of a Sketch of a Circular Orifice.

Partially submerged orifice, also known as partially drowned orifice, is an orifice with its discharge side situated under a partially submerged condition as shown in Figure 1.2. It consists of two parts, i.e. an upper portion and a lower portion, whereby the approach side act as a free discharging orifice while the discharge side behaves as a submerged orifice. Therefore, the total discharge flow is the summation of flows from both portions (Karki, 2018). In this project, correlation study of circular orifice in a partially submerged condition is obtained via CFD simulation using ANSYS Fluent. Albeit considerable research with similar topics have been conducted, majority is carried out using rectangular orifice, but lack of study on circular orifice. Thus, this study aims to provide insight into using circular orifice in partially submerged condition.

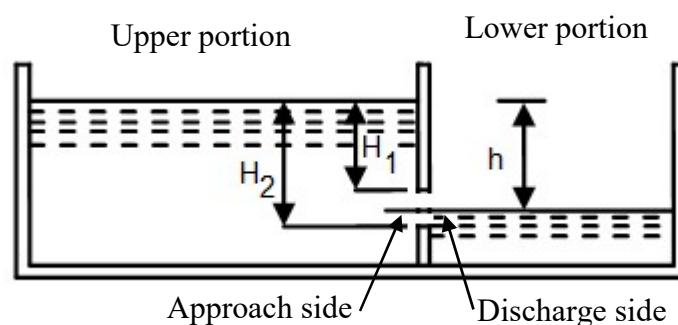


Figure 1.2: Partially Drowned Orifice (Ahmad, 2012).

1.2 Importance of Study

Hussain and Haroon (2019) states that from the flow management point of view, knowledge regarding the flow mechanics of an orifices is necessary, so as to be able to distribute discharge from channel with greater effectiveness and accuracy. Estimation of the discharge nature as well as accurate determination

and specification of the precise processing parameters are extremely important for the operation and maintenance of water drainage system and stormwater management. Even though water industries often operates under partially submerged conditions, the partially submerged orifice flow seems to be forgotten if compared with the conventional flow through free discharge orifice and submerged orifice. In fact, majority of the operation for stormwater detention facility are under partially submerged conditions even though the orifice structures was designed to cope with runoff flow control under submerged condition (Guo and Urbonas, 1996). Therefore, this study may provide insight regarding the hydraulic behaviour of partially submerged orifice flow for industries that deals with the design and construction of water work infrastructures as well as runoff flow control in stormwater management. Example of water industries application includes the construction and commissioning of water treatment plant and raw water intake plant.

1.3 Problem Statement

The common orifice employed for water conveyance from source to alternative channels are rectangular and circular orifice (USBR Water Measurement Manual, n.d.). Figure 1.3 illustrates the flow diversion structure of a free discharging orifice (A) and partially submerged orifice flow (Case B and C) in open channels. **Case A** is the most classic orifice flow, which it requires only the upstream head to determine the flow rate via Bernoulli Principle. Both **Case B** and **C** are partially flooded with a free surface flowing downstream, but with a difference of upstream water surface. In a water-filled open tank, the dominant driving force for the liquid flow through orifice would be the difference in water levels. The study regarding partially submerged orifice flow was found to be minimal, with zero research regarding the application of simulation processor to describe the flow behaviour. Therefore, the aims of this project is to determine the correlation of volumetric flow rate with the orifice dimension of orifice diameter and water level difference for a partially submerged circular orifice flow. The aforementioned parameters of interest was illustrated in Figure 1.4.

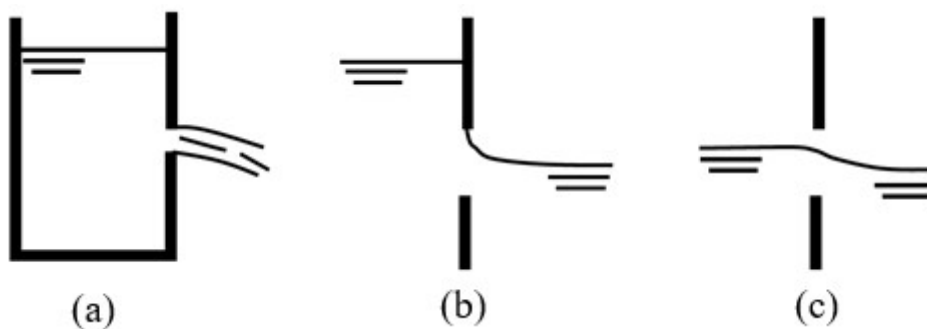


Figure 1.3: Orifice Flow, (a) Free Discharging, (b) Orifice Outlet is Partially Submerged, (c) Both Sides are Partially Submerged

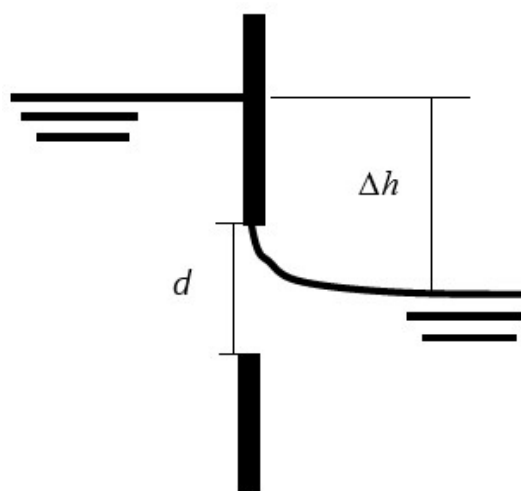


Figure 1.4: Parameters of Interest.

1.4 Aim and Objectives

The main aim of this project was to obtain the correlations for **Case B** and **C**. The following are the specific objectives that must be completed in order to achieve the main aim:

- i. To develop Computational Fluid Dynamics (CFD) simulation for **Case A, B** and **C** using ANSYS Fluent.
- ii. To validate the CFD model developed using **Case A**.
- iii. To perform correlation studies for **Case B** and **C**.

1.5 Scope and Limitation of Study

Variables that correlates with the discharge performance of partially submerged circular orifice is investigated. The study includes full 3-dimensional (3-D) problems covering **Case A, B** and **C** along with a base model of 2-dimensional

(2-D) for **Case A** using CFD software. The validation for **Case B** and **C** was not covered in this study due to lack of experimental data. Furthermore, external forces, such as wind velocity and wave propagation were not accounted in this study. Instead, this study focus on the open channel flow that is driven by gravity and inertia, thus gravitational acceleration of -9.81 m/s^2 is assumed. In addition, the bottom wall effect at the downstream was neglected, as the vessel floor is assumed to be located in a sufficient far distance, having zero external influence, hence was set as symmetry in the boundary condition. It is also important to note that the study assumes that all flow regime are turbulence and thus laminar model is not included in the simulation environment. This assumption was also in accordance with Section 2.2 under literature review in Chapter 2, where turbulence models were implemented for all the CFD simulations reviewed.

CHAPTER 2

LITERATURE REVIEW

2.1 Orifice Flow

According to Eghbalzadeh, et al. (2016), the typical variables that affects the outcome flow pattern of an orifice are the geometry and hydrology parameters, including the type of orifice shape, orifice opening parameters such as orifice diameter and thickness of orifice as well as the upstream water level, crest height and fluid velocity. Using constricted flow methods, hydraulic parameters of the orifice can be obtained by specifying one or two constriction on dimensions and craftsmanship (Taghvaeian, n.d.). Pre-specified dimensions refers to the shape and size of orifice that are closely simulate to the existing condition. When performing calibration to determine the flow rate, the known dimensions are substituted into the respective orifice equation depending on the operating condition. In the theoretical equations, hydraulic coefficients that account for the discharge velocity reduction caused by contraction and friction, as well as the neglect of approach velocity head and velocity distribution are applied to remove all deviation from ideal condition (USBR Water Measurement Manual, n.d.). Among the coefficients stated above, the standard convention for most researchers to investigate the hydraulic structures such as orifice is by using the coefficient of discharge.

Coefficient of discharge is defined as the ratio of actual discharge to the theoretical discharge, at which it predominantly determines the flow pattern of an orifice. With discharge coefficient close to unity of 1, it implies that the orifice flow is approximating to an ideal discharge with zero energy losses. However, the law of thermodynamics restrict the discharge coefficient to be 1 in the practical world. For discharge coefficient to be unity of 1, it is only possible with the assumption of zero pressure at the gate opening and negligible surface tension and friction effect of the fluids, at which it is impossible to achieve in real life.

Unlike the orifice plates in pipe flow, at which the dominant driving force is pressure gradient, the only driving force for an orifice flow in open channel is gravitational and inertia force. Swamee, et al. (1993) conducted an

analysis to find the discharge relationship through a side sluice, by studying the effect of discharge coefficient to the gate length. In an open channel flow, the authors verified the relation of main channel flow depth and gate opening to the discharge coefficient. Ramamurthy, et al. (1987) investigated the correlation for weir-orifice discharge under uniform flow distribution and concluded that the weir-orifice unit can be constructed to produce an outflow with prescribed percentage of inflow under a variation of flow depth of upstream. They also proven the approach Froude number to be an important parameters to discharge coefficient. This is in line with the work from Singh, et al. (1994), Borghei, et al. (1999) and Ghodsian (2003) which concludes Froude number as well as the flow depth to weir height ratio as the parameters for discharge coefficient. In the present study, the discharge coefficient of the free discharging orifice (**Case A**) were reviewed and extracted from the journal, regardless from equations or just specific values, to validate the CFD model developed. The model or value referred for this study were presented in the upcoming subsection. Furthermore, journals regarding the background and theories for **Case A, B** and **C** will also be included in the sections below.

2.1.1 Free Discharging Orifice Flow

The fluid flow pattern of a free discharging orifice is commonly presented as a modular flow when the fluid is discharged into free air. Figure 2.1 illustrates an example of free discharge flow through a sharp-edged orifice to free air, producing a contracted jet due to the restriction of cross sectional area. Jet contraction will only occur if there is sufficient upstream water head to convert all the approaching water streamlines from all directions to the orifice. The formation of jet contraction is also limited by the presence of external force since it will disrupts the direction of discharge flow. Vena contracta is referred to the section with maximum jet contraction with approximately half the orifice diameter (Bos, 1989). Bos (1989) and (Ratnayaka, et al. (2009) state that the common equation, to relate the pressure and velocity in a free discharging orifice is by the derivation of the Bernoulli's theorem as shown in Eq.(2.1). The formulation of the conventional equations for discharge velocity and volumetric flow of free discharging orifice flow is presented by Eq.(2.2) and Eq.(2.3). Typical discharge coefficient for a sharp-edged opening or a fully contracted,

submerged, rectangular orifice is around 0.61 according to both Bos (1989) and (Ratnayaka, et al. (2009).

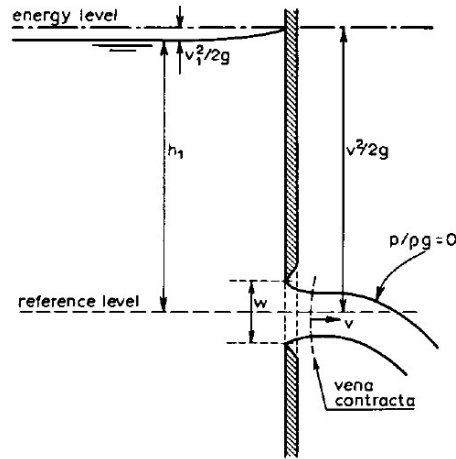


Figure 2.1: Free Discharging Orifice (Bos, 1989).

$$h = \left(h + \frac{v_1^2}{2g} \right) = \frac{v^2}{2g} \quad (2.1)$$

$$v = \sqrt{2gh} \quad (2.2)$$

$$Q = C_d A \sqrt{2gh} \quad (2.3)$$

where Q is the volumetric flow rate, C_d is the discharge coefficient, A is the orifice area, g is the gravitational acceleration and h is the average head as shown as h_1 in Figure 2.1.

On the other hand, by substituting the area of circular orifice in terms of orifice diameter, d into Eq.(2.3), the discharge equation for a small sharp-crested circular orifice in open channels is presented as in Eq.(2.4), (Swamee and Swamee, 2010; Hussain, et al., 2010)

$$Q = \frac{\pi}{4} C_d d^2 \sqrt{2gh} \quad (2.4)$$

The discharge coefficient for free discharge flow through circular orifice is dependent on the diameter of orifice, d . Assuming negligible approach

velocity, the average discharge coefficient for circular orifice in free discharge flow is shown in Table 2.1.

Table 2.1: Average Discharge Coefficients for Free Flow through Circular Orifice (Bos, 1989).

Orifice diameter, d (mm)	C_d
20	0.61
25	0.62
35	0.64
45	0.63
50	0.62
65	0.61
≥ 75	0.60

USBR Water Measurement Manual, (n.d.) states that the contraction of orifice can be divided into two type, where one is the formation of jet contraction near the opening of orifice as shown in Figure 2.1 and the other would be zero curvature of jet passing through the orifice, also known as the sluice gate, as illustrated in Figure 2.2. The undershoot gate of sluice gate is formed when water discharges freely through an orifice with the contraction of both side and bottom suppressed. According to Bos (1989), sluice gate is a half-model of a two-dimensional jet, whereby the plane of symmetry of the jet is substituted by the bottom channel of the sluice gate. Therefore, the flow through sluice gate is determined using the same discharge equation as the free discharge orifice, which is Eq.(2.3).

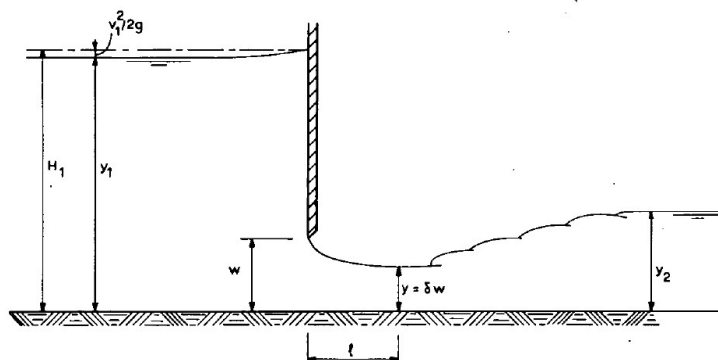


Figure 2.2: Flow Past Sluice Gate (Bos, 1989).

According to Bos (1989), the discharge coefficients for free flow under sluice gate was found to be around 0.596 to 0.605 depending on the ratio of water depth to the opening size. The results tally with the research done by Kim (2007), where he summarised the existing investigations and knowledge on gates from both theoretical and experimental studies. By doing so, the discharge coefficient was found to be around the range of 0.595 as shown in Table 2.2. The last row of the table represents the CFD results on sluice gate from Kim (2007) whereas the others are experimental investigation by authors of Rajaratnam and Subramanya (1967), Nago (1978) as well as Roth and Hager (1999).

Table 2.2: Summary of Discharge Coefficient for Flow under Sluice Gate.

Authors	C_d
Rajaratnam and Subramanya (1967) (Experimental)	0.595
Nago (1978) (Experimental)	0.520-0.595
Roth and Hager (1999) (Experimental)	0.492-0.594
Kim (2007) (Experimental)	0.506-0.598

Hussain, et al. (2011) performed a research to examine the probable variables that affects the discharge coefficient of a rectangular side orifice in open channel. Discharge equation, Eq.(2.3) is only applicable for small opening with constant pressure distribution over the flow area, where the orifice opening is parallel to the incoming flow, according to Ojha and Subbaiah (1997). For the case of side orifice, as studied by Hussain, et al. (2011), where the flow direction is perpendicular to the orifice opening and pressure head varies over the flow area, the discharge equation is represented by Eq.(2.5). (Chadwick, et al., 2004; Doughlas, et al., 2005)

$$Q = C_d \sqrt{2g} \frac{2}{3} L \left(H_{1r}^{\frac{3}{2}} - H_{2r}^{\frac{3}{2}} \right) \quad (2.5)$$

where L is the width of rectangular orifice, H_{1r} is the water level from the bottom orifice and H_{2r} is the water level from the top of orifice as shown in Figure 2.3.

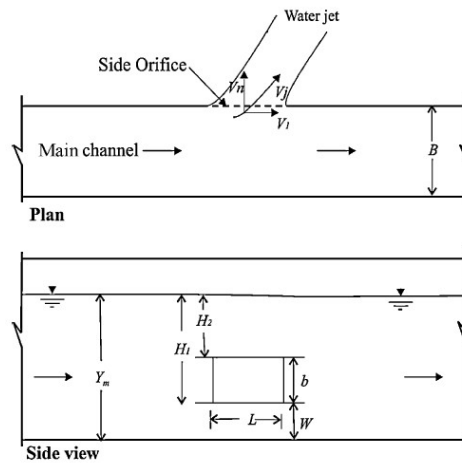


Figure 2.3: Rectangular Side Orifice under Open Channel Flow (Hussain, et al., 2011).

Furthermore, Hussain, et al. (2011) compared his experimental studies on the investigation of the open channel flow through circular side orifice in 2010 and rectangular side orifice in 2011. Both orifices are evaluated under the same opening area, geometry and flow characteristics. Discharge coefficient was utilised as the indicator to determine the orifice's efficiency, at which higher discharge coefficient would leads to greater efficiency. The results of comparison was illustrated in Figure 2.4.

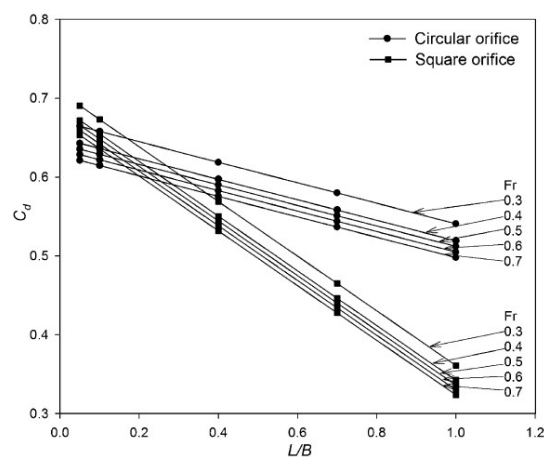


Figure 2.4: Variation of Discharge Coefficient for Circular and Rectangular Side Orifices with Different L/B or D/B (Hussain, et al., 2011).

On the x-axis of Figure 2.4, B represents the width of main channel as shown in Figure 2.3. Based on Figure 2.4, the relationship between parameters were established with two validated hypothesis stating: (a) discharge coefficient is increases when Froude number decreases for constant L/B ; (b) discharge coefficient is inversely proportional to L/B at a given Froude number, which was assumed to be caused by the presence of boundary effect from the opposite channel wall. Hypothesis(a) is in line with the relationship established for flows through weirs or sluice by Singh, et al. (1994) and Borghei, et al. (1999). Furthermore, analysing the graph above, the circular orifice is superior to rectangular orifice when L/B is greater than 0.2 and vice versa. The symmetry circular jet produced in circular orifice flow leads to a higher discharge coefficient whereas the inward force built in the pressure of vena-contracta in rectangular orifice is greater, hence lower discharge coefficient (Hussain, et al., 2011). Therefore, the work of Hussain, et al. (2011) proves that the efficiency of circular orifice in open channel is greater for a thin walled circular orifice with high orifice diameter.

Moreover, orifice can be classified as small or large orifice and the difference between small and large orifice depends on the head of fluid from the orifice center as shown in Figure 2.5. To explain further, for an orifice diameter (d) that is five times less than upstream water-head (h), the orifice is considered as a small orifice and vice versa for large orifice (Thajudeen, 2018). Kubrak (2015) published a research paper assessing the theoretical aspects of small and large unsubmerged circular orifices in steady water flow estimation using variable headwater-diameter ratio. Through analytical derivations, the discharge equation for small and large orifices was formulated and the results obtained was compared with each other. The author proved that the discharge characteristics along with the discharge rate for both orifices are identical when $h \geq 4d$. Yet, significant deviation occurred when the headwater-diameter ratio is 0.5, accounting for 4 % of percentage difference between the discharge of small and large orifice. He concluded that the percentage deviation would reduce to zero once the water surface level increases to a certain extent (Kubrak, 2015).

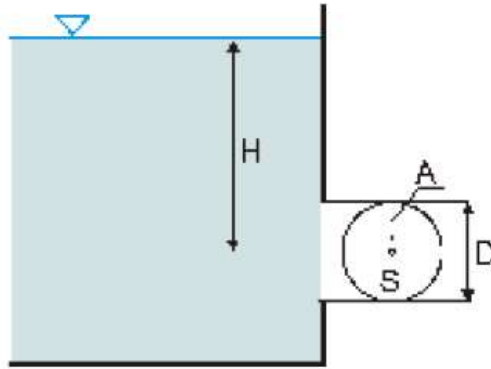


Figure 2.5: Steady Free Surface Flow through Circular Orifice (Kubrak, 2015).

Water control gates are divided into undershoot gate and overshoot gate. The former represents the sluice gate as discussed earlier while the latter is akin to the flow over a weir as shown in Figure 2.6 (Ratnayaka, et al. (2009). The discharge equation for weir flow is the classic Rehbock formula as shown in Eq.(2.6) Eq.(2.7) and Eq.(2.8) (Oshima, et al., 2013).

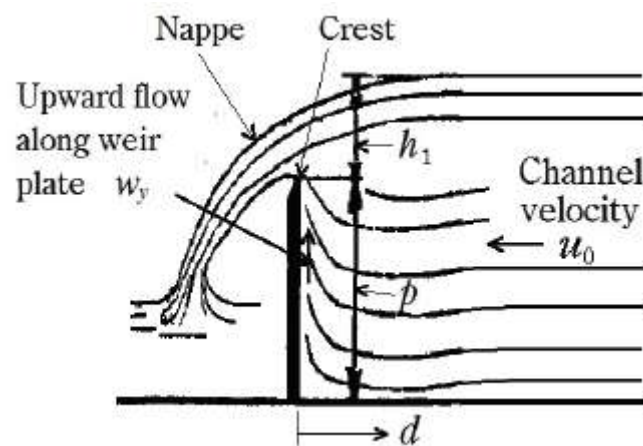


Figure 2.6: Flow over Sharp-crested Weir (Oshima, et al., 2013)

$$Q = C_d \frac{2}{3} \sqrt{2g} b h_e^{\frac{3}{2}} \quad (2.6)$$

$$C_d = 0.6035 + 0.0813 \frac{h_1}{p} \quad (2.7)$$

$$h_e = h_1 + 0.0011 \quad (2.8)$$

where Q is the volumetric flow rate, C_d is the discharge coefficient, g is the gravitational acceleration, b is the width of weir, h_{le} is the effective weir head, h_l is the measured weir head and p is the weir plate height as illustrated in Figure 2.6. According to Oshima, et al. (2013), the Rehbock formula is specified in International Organization of Standardization, ISO 1438:2008, where it was verified and restricted for weirs with weir plate height, p of less than 1 m. By that, the formula is suitable for to be used for the CFD model in this study since the geometry of the model fulfills the requirement above.

2.1.2 Partially Submerged Orifice Flow

Guo and Stitt (2017) concluded a weighting factor model that provides promising data in accordance to low-flow hydraulics through circular orifice, which may be helpful in coping with runoff flows of full spectrum. The headwater-to-diameter ratio was employed as the submergence fraction of a circular orifice to determine the mixing flow in the model. The authors proposed a design condition for partially submerged circular orifice flow which includes the following,

- (1) The invert of orifice must be at least one diameter less than the upstream headwater depth.
- (2) Negligible tailwater effects are assumed with full jet contraction.

The aforementioned design condition allows the partially submerged flow problem to be associated with the parameters as shown in Figure 2.7.

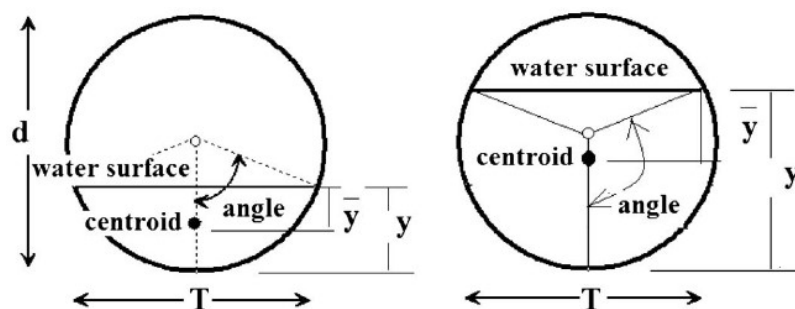


Figure 2.7: Partially Submerged Flow in Circular Orifice (Guo and Stitt, 2017).

Guo and Stitt (2017) formulated two equations for partially submerged circular orifice flow and partially submerged circular weir flow. Combining the

equations, a rating curve equation was formed using the weighting factor to estimate the transition flow from a partially submerged circular weir flow to an orifice flow, in the range of $0 < y/d < 1$. The equation was also suggested to apply Froude number as a form of normalization and discharge coefficient as a basis for calibration. To summarise the literature written by Guo and Stitt (2017), the observed data fits perfectly with the normalised partially submerged orifice flow using the aforementioned equation and the optimal discharge coefficient, C_d was examined to be 0.53.

However, the work of Guo and Stitt (2017) was questioned by Vatankhah (2018), at which there presents methodological contradictions in constructing the equations for partially submerged circular orifice flow and transition flow. He explained that unlike the cross-sectional area for circular weir flow, where the values are variable, and the orifice cross-sectional flow area is not subjected to change. Hence, the range of $0 < y/d < 1$ used by the authors in partially submerged circular orifice flow was not applicable. Defining the submergence fraction with respect to the type of flow, the circular channel would resemble a fully submerged orifice flow if $y/d \geq 1$ whereas for partially submerged case, it is similar to a weir under the range of $0 < y/d < 1$. Contrary to expectations, the transition flow from shallow-water weir flow to a deep-water orifice flow for a circular opening is not possible because there is absence of orifice flow in the range of $0 < y/d < 1$. Estimation for transitional flow is only feasible at the approximate point where y/d is equal or close to 1 as shown in Figure 2.8 (Vatankhah, 2018).

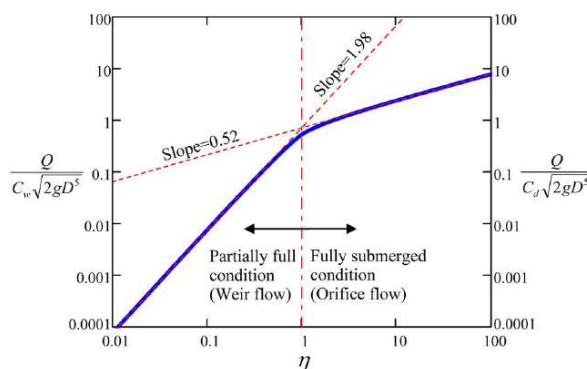


Figure 2.8: Dimensionless Headwater-to-diameter Relation for a Fully Submerged Circular Orifice Flow and Partially Full Circular Weir Flow (Vatankhah, 2018).

Based on the Figure 2.8, it can be explained that the orifice will act as a circular weir provided the fluid flow through orifice exceeds the critical depth under partial submergence condition. Using the same weighting factor method and headwater-to-diameter ratio, Vatankhah (2018) modified the equations under the literature of Guo and Stitt (2017). He formulated a discharge equations which is applicable for full-range circular openings flow that unifies both weir flow to orifice flow. The equation includes both discharge coefficients of orifice flow, C_d and weir flow, C_w with values calculated from experimental data. Theoretically, both coefficients should be equal at the transition point, yet it is unlikely to happen in practical. Therefore, the presence of discontinuity will be estimated near the transition point, approximating to baffle-sluice gates. Nonetheless, the author proposed the equation can be used to model the hydraulic behaviour of broad-crested and sharp-crested opening channels for relevant industrial applications.

Brandes and Barlow (2012) developed two possible models of top-width weir and equivalent-area weir for flow rate prediction in thin-walled orifice flow under partially submerged conditions. The models proposed was formed by treating the partially submerged orifice as a rectangular weir with equivalent size. To validate the approach models, thin-walled circular orifice with 5 cm to 10 cm are tested under two experiments including steady-state flow versus stage experiment and transient drainage experiment. The former experiment is performed by continuously draining and filling of the flumes, allowing the inlet and outlet of the fluid flow to achieve steady state whereas the latter experiment replicates the model of the rainwater retention basins or storage lakes, at which fluid was stored in a vessel before draining through the hydraulic structure. Since the two models developed in the paper treats partial submergence as flow through circular weir, the circular weir model by Bos (1989) as stated below was implemented and compared with the results obtained.

$$Q = C_e \omega \frac{4}{15} \sqrt{2gd^{2.5}} \quad (2.9)$$

where C_e is the effective discharge coefficient, ω is the filling ratio of h_1/d , h_1 is the weir head and d is orifice diameter. For clearer understanding of the parameters involved, Figure 2.9 can be used to refer, where D is equivalent to d and h_w is the h_1 from Eq.(2.6).

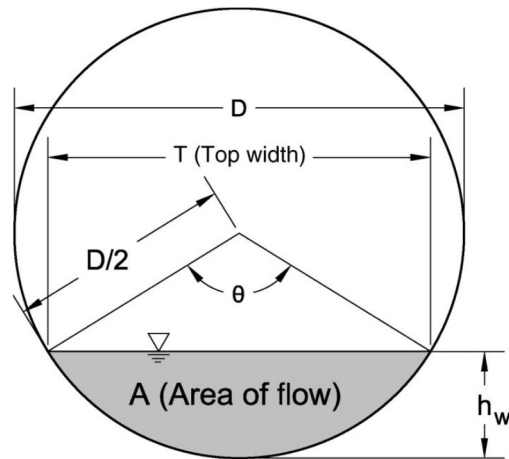


Figure 2.9: Schematic of a Partially Submerged Orifice (Brandes and Barlow, 2012).

The experiment was carried out in a horizontal flume with an orifice experimental setup allowing the full demonstration of orifice flow. Different from allowing the water to flow freely in our study, pumps was used in the experiments carried out by Brandes and Barlow (2012), so to achieve the desired flow rate. Nevertheless, the parameters of orifices tested by Brandes and Barlow (2012) are presented in the table below,

Table 2.3: Parameters of Orifice Tested (Brandes and Barlow, 2012).

Orifice	Diameter, D (cm/in)	Thickness, l (in)	Material
1	10.16 / 4.0	0.17	Sheet metal
2	7.79 / 3.06	0.16	Sheet metal
3	5.23 / 2.06	0.31	Sheet metal

Results of the experiments of the two models are compared with experimental model as well as the Bos, 1989 model. For the steady-state experiments, graphs of the flow rate against the headwater-to-diameter ratio was

plotted as shown in Figure 2.10. The abbreviations used for variables in x-axis of headwater-diameter ratio (h_w/D) is rather different from Guo and Stitt (2017) (y/d), yet they both implies the same parameters. Under the graph legend, the third row represents the top-width weir model whereas the fourth row is the equivalent-area weir model.

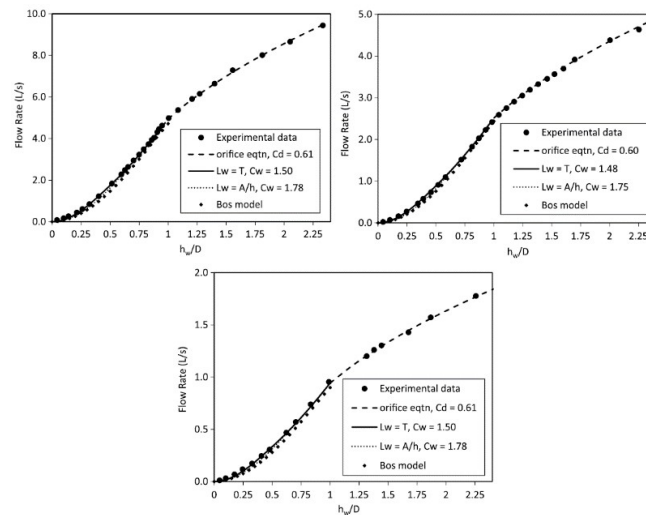


Figure 2.10: Comparison of Model in Steady-state Experiments: Top left (Orifice 1), Top Right (Orifice 2), Bottom (Orifice 3) (Brandes and Barlow, 2012).

Based on the figure above, it can be observed that the Bos (1989) model, consistently underpredicts the outflow data from the experiment, proving the two models proposed in this study gave better fit performance. Yet, top-width weir model shows better agreement to the experimental data if compared to the other equivalent-area weir model. When the fractional submergence is greater to 1, all three models were not matched or fitted due to the flow-matching boundary constraint in submerged orifice flow. Although it was not mentioned in the journal, a hypothesis can be made regarding the dependency of flow rate on orifice diameter. By analysing all three graphs, it is clear that the flow rate increases as the diameter of the thin-walled orifice increases, despite the increment change in diameter ratio. At the same diameter ratio, the influence of the orifice diameter towards the flow rate is greater than the headwater. This is in line with Eq.(2.4), at which the relation of orifice diameter in the discharge equation is in the second order if compared to the headwater.

The subsequent transient drainage experiments by filling the flume and allowing the fluid to be freely drained afterwards. The results of the experiments is seen in Figure 2.11,

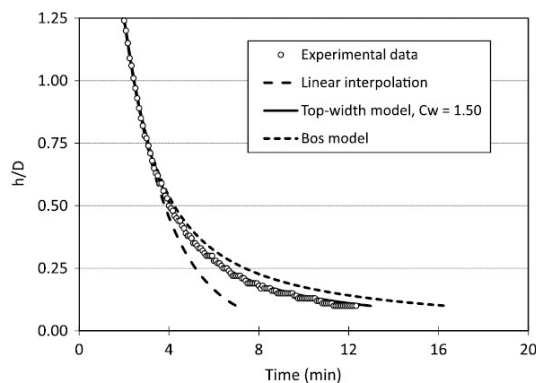


Figure 2.11: Transient Drainage Experiments with Orifice 1 (Brandes and Barlow, 2012).

By observing the graph above, when the orifice displays full submerged flow ($y/d > 1$), all model curves are identical. From the experiments conducted. Brandes and Barlow (2012) concluded that the proposed top-width model provides the best fit for accurate modelling of thin-walled partially submerged orifice flow. In the subsequent paper, Barlow and Brandes (2015) conducted the same experiments but with the aim to investigate the applicability of the empirical models to thick-walled concrete orifices, for practical detention basin structures. Apart from the equivalent rectangular weir used in the previous paper, addition models of the Storm Water Management Model (SWMM) and the Virginia Tech/Penn State Urban Hydrology Model (VTPSUHM) were incorporated in the new study. For partially full flow of the concrete orifice, equivalent rectangular weir model exhibits the lowest average absolute error, with 6.71 %, proving to be the best fit to the experimental data if compared to other two models (Barlow and Brandes, 2015).

2.2 CFD Modelling for Orifice and Open Channel Flow

In this study, several design parameters were to be tested in a CFD modelling software. The ease of the software to sketch and manipulate the orifice geometries and parameters provides exceptional advantages in terms of time and

costs, over the conventional experimental method. Unlike the experimental approach, the physical hydraulic structures of an orifice flow model is not required in the computational fluid dynamics study. CFD is a high-fidelity predictive software that was commonly devoted to model the flow behaviour of water particles in orifice flow. The application of CFD in the modelling of flow pattern through orifice has gained momentum due to the increase in the interest in the utilisation of orifice in irrigation engineering. In fact, a significant amount of researchers have published their study regarding the CFD study in orifice flow, especially for rectangular orifice. CFD technology is superior to the conventional physical experiments, in terms of cost reduction, rapid data assessment and response, promising flexibility that allows the user to simulate various conditions as well as to examine and interpret the performance in any location under the region of interest without interruption (Pretechnologies, 2020). That is to say, although the present study could be conducted using an experimental approach, but the complexity in terms of geometry and operating conditions in this project tends to shift towards using the CFD simulation method to obtain the analytical relationship. With these advantages, results obtained from CFD study can be analysed to cope with supporting decisions in risk and safety management of the operating assets. However, the numerical tool is not perfect and 100 % reliable as the outcome is very much dependent on the model setup. The digital computation may inherent numerical errors that influence the accuracy and precision of the results, leading to a non-ideal convergence of results data. Therefore, a mesh independence study is often performed to ensure the independency of the mesh resolution to the solution and prevent erroneous results. Moreover, one of the disadvantage of CFD software is the complexity within its calculations, causing it to become processor-intensive. Hence, more complex model would imply the requirement of substantial modelling cost and computational time to simulate the solutions (Peritus, 2019).

The present study involves free surface operating condition. Free surface problems are exceptionally difficult and tricky to simulate as the water flow tends to be unstable with frequent fluctuations. Owing to the unsteadiness of the flow, convergence issue may exists when performing the calculations for the simulation if the convergence residuals are set according to the normal standard.

Therefore, the convergence criteria of a free surface flow can be increased to two orders of magnitude higher than the conventional values for monitor residuals as depicted in Table 2.4 (Datawave Marine Solutions, 2019). Nevertheless, the following subsections includes all CFD study regarding orifice flow and open channel flow.

Table 2.4: Guideline for Monitor Residuals (Datawave Marine Solutions, 2019).

Monitor Residuals	Description
1×10^{-3}	Acceptable result, but not very reliable.
1×10^{-5}	Excellent, reliable result.
1×10^{-6}	Insane quality but not necessary.
For free surface flows, multiply 1×10^2 to all levels.	

2.2.1 Turbulent Overflow on Stepped Spillways

Chen, et al. (2002) conducted an analysis to study the feasibility of $k-\varepsilon$ turbulence model in describing the hydraulic performance of a free-surface stepped spillway overflow. By experimenting the turbulence numerical simulation with Volume of Fluid (VOF) method as well as unstructured grid, the author successfully displayed an identical outcome with measured data, where the velocities and pressure are well compared. The study concludes the effectiveness of using $k-\varepsilon$ turbulence model to simulate free-surface problems.

2.2.2 Free Flow Past a Sluice Gate

Kim (2007) utilised a computational fluid dynamic program FLOW-3D to model the fluid flow past sluice gate. The main objective of the study was to determine the contraction and discharge coefficients as well as the pressure distribution using the Reynolds averaging Navier-Stokes equations (RANS), which was numerically solved using CFD program via the finite-volume approach. Similar to the work done by Yu, et al. (2013) and Chen, et al. (2002), the tracking of the free surface was done by implementing the VOF method. However, for turbulence closure, the Renormalised $k-\varepsilon$ turbulence model (RNG $k-\varepsilon$ model) was selected due to its accurate modelling of flows having low intensity turbulence and strong shear regions. In comparison with the

experimental data, the study ends with good agreement in terms of pressure distribution and discharge coefficients, which range from 0.506 to 0.598 in values.

2.2.3 Side Weir Flow in Open Channel

Mangarulkar (2010) performed an experimental and CFD study on the characteristics of side weir flows under free surface condition. In his work in simulation model, the 3-D multiphase model was constructed by VOF scheme with finite volume approach (FVM) to simulate the side weir problem. RNG $k-\varepsilon$ turbulence model was employed as the viscous model so to simulate the turbulence behaviour of the model. For the solution method, Pressure Implicit with Split Operator (PISO) scheme was selected as the pressure-velocity coupling method with pressure staggering option (PRESTO!) as the pressure discretization scheme. Based on the simulation results, Mangarulkar (2010) concluded that the results shown good agreement with experimental results.

2.2.4 Free Surface Flow over Triangular Labyrinth Side Weir

Aydin (2012) investigated the feasibility to model free surface flow over triangular labyrinth side weir by using CFD simulation through High Performance Computer (HPC). The study was a success, at which the flow characteristics of the complex problem in free surface turbulent flow can be determined through ANSYS-Fluent using VOF method and open channel boundary conditions. In the subsequent publish, Aydin and Emiroglu (2013) performed a CFD analysis to determine the factors that affect the discharge capacity using the same CFD model. Both studies were compared with the experimental results from Emiroglu, et al. (2010), where reasonable agreement was observed in comparing both journals with measured data. Furthermore, Aydin (2012) as well as Aydin and Emiroglu (2013) conducted a comparative study to determine the most competent turbulence model to be used before proceeding to the part of CFD analysis. Five turbulence models were included in the comparison section, which are Spalart-Allmaras model (a), $k-\omega$ model (b), standard $k-\varepsilon$ model (c), RNG $k-\varepsilon$ model (d), realizable $k-\varepsilon$ model (e) and Reynolds Stress Model (RSM model) (f). Figure 2.12 and Figure 2.13 represent the respective criteria to be judged in determining the most effective turbulence

model in both journals. By that, RSM model was found to be most suitable model to simulate the surface shapes of the complex flow that involves simultaneous surface fluctuations and vortex formation.

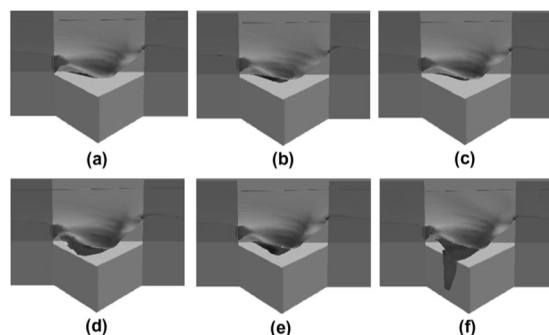


Figure 2.12: Comparison of Different Turbulence Models with Surface Profiles of Vortex Formation inside Triangle Labyrinth Side Weir (Aydin, 2012).

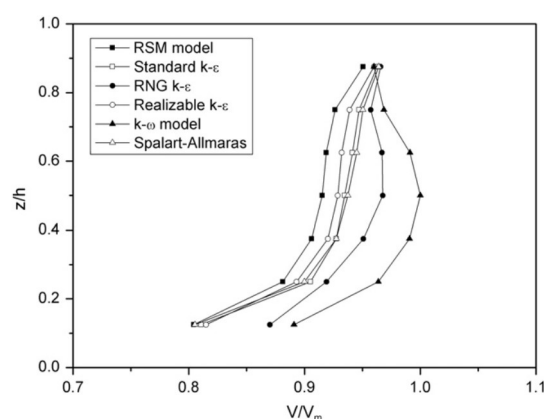


Figure 2.13: Determining the Sensitivity of Results for Different Turbulence Models (Aydin and Emiroglu, 2013).

2.2.5 Free Surface Flow over Side Weir

Mahmodinia, et al. (2012) conducted a CFD simulation via Fluent 6.30 program to study free surface flow over sharp crest side weir under the effects of different upstream Froude number. Under the author's CFD simulation, Reynolds Stress Model (RSM) was employed as viscous model and the VOF method was chosen to simulate the free surface. The following settings was applied in the Solution Mehods panel for the simulation of free surface flow over side weir,

- Pressure velocity coupling method: PISO algorithm scheme
- Discretisation scheme for pressure : PRESTO!

- Discretisation scheme for momentum : Quadratic Upstream Interpolation for Convective Kinematics (QUICK)
- Discretisation scheme for turbulent kinetic energy : First order upwind
- Discretisation scheme for turbulent dissipation rate: First order upwind

For iterative solutions, the absolute convergence criteria was set to at least three orders of 0.001 for all equations whereas for transient solver, it was set to four orders of 0.0001 with time step size of 0.01s. From the simulation results, Mahmoodinia, et al. (2012) concluded that the increment of Froude number shifts the separation zone area towards the downstream end.

2.2.6 Orifice Flow in a Trough-type Liquid Distributor

Yu, et al. (2013) have proven the application of CFD simulation is feasible in describing the orifice flow through trough-type liquid distributor. An experiment setup was used to represent a simplified trough-type liquid distributor. In the objective for validation of CFD simulation, the observed results are compared with the simulated results. Discharge coefficient was used as the parameters to evaluate both results and they are calculated via Eq.(2.4). The influence of lateral flow to the orifice flow was demonstrated through visual analysis of the velocity vector and pressure distribution diagram from ANSYS software. Figure 2.14 illustrates the computational domain designed by Yu, et al., 2013, at which it includes a 770 mm × 30 mm × 240 mm vessel with 10 orifices of 8 mm diameter and 2 mm thickness casted in its side wall.

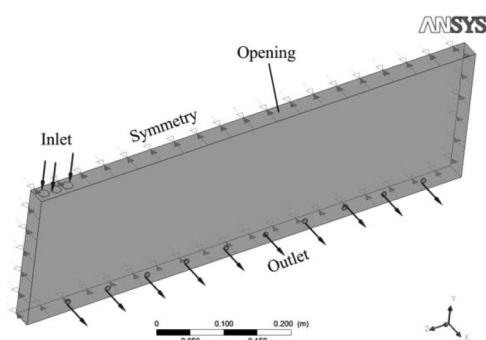


Figure 2.14: Sketch of Orifice Flow in Through-type Liquid Distributor (Yu, et al., 2013).

Various assumptions are considered in the simulation work, including no slip condition, zero relative pressure for outlet and opening as well as the operating condition of room temperature and atmospheric pressure. In the context of meshing application, unstructured meshes was used instead of the structured meshes. The combination of prismatic and tetrahedral grid was employed, at which the former sorts out for orifice wall and the latter accounts for all other locations. Similar to Hussain and Haroon (2019), the mesh at vicinity of orifice was refined to provide an accurate description of the orifice flow. To establish that the model is not influenced by mesh size, mesh independence study was carried out. In the solution setup, volume-of-fluid (VOF) method and shear stress transport (SST) turbulence model was employed as the multiphase model and viscous model, respectively. VOF method is well-known in tracing the interface of water and air whereas the SST model provides accurate flow estimation. For the solution panel, coupled algebraic multi-grid method was selected as the iteration solution method. The convergence absolute criteria in terms of root mean square residual was set to 0.00001, in which the value was proven to be sufficient to obtain the converged results with promising accuracy (Ansys, 2009). In this paper, ANSYS CFX software was used because of its outstanding performance in simulating free surface treatments.

The experimental results tested with 0.776 kg/s and 1.26 kg/s inlet flow and simulation results using the inlet flow of 0.388 kg/s and 0.63 kg/s were compared with discharge coefficient as y-axis. Figure 2.15 illustrates the results comparison of lower inlet flow in the left whereas the right graphs covers the results with higher flow rates. Both sets of results show good agreement in terms of discharge coefficient.

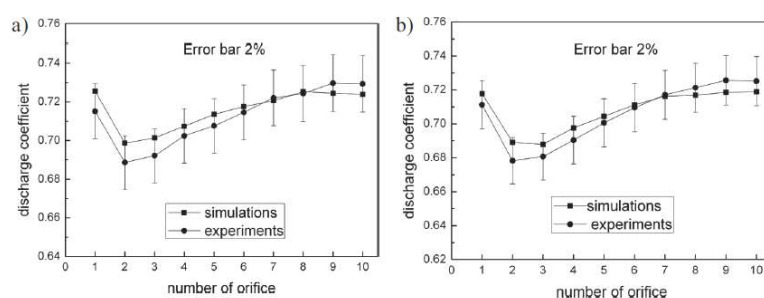


Figure 2.15: Comparison of Observed and Simulated Results (Yu, et al., 2013).

From the CFD simulation done by Yu, et al. (2013), the velocity vector distribution demonstrates a decreasing trend of fluid velocity from orifices 1 to 10 and the formation of high flow velocity regions around orifices 2 to 4, as shown in Figure 2.16. The descending velocity vectors are attributed to the continuous discharge of flow for every time the liquid passes through the orifice. Orifice 3 is located under the high velocity flow region, at which the discharge of that particular is influenced the most from lateral flow. As approaching fluids enters orifice 3 from nearest side of the orifice, the entering of orifice was prevented by lateral flow in the further side of the orifice. This is due to concept of the conversion of kinetic energy to hydrostatic pressure and vice versa. At the entering zone of the orifice, the hydrostatic pressure is converted into kinetic energy, forming low static pressure which approximates to a hemispherical zone where fluids are forced to be discharge out the orifice. Other fluids that past the hemispherical region are affected by lateral flow, leading to the formation of high static pressure which hinders the flow to enter the orifice. By the influence of lateral flow, the velocity and pressure distribution at the particular orifice is disrupted, causing a decrease in discharge coefficient as shown in Figure 2.15. Based on Figure 2.15 and Figure 2.16, it can be observed that the effect of lateral flow gradually reduces from orifices 2 to 10.

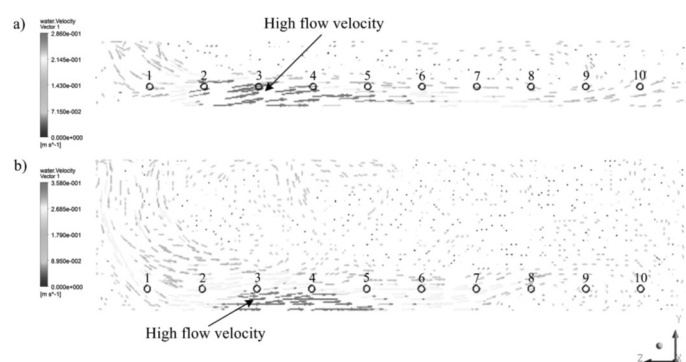


Figure 2.16: Velocity Vector Distribution for 0.388 kg/s Inlet (a) and 0.63 kg/s Inlet (b) (Yu, et al., 2013).

Despite changing the model geometry, a strategy was proposed by Yu, et al. (2013), which includes increasing the distance between orifice. The author's estimation of the strategy outcome was that increasing the distance of

orifice center to trough bottom would ultimately reduce the influence of lateral flow to minimum. With such expectation, the authors successfully proven the theory by CFD simulation with 3 variable distances of 30 mm, 45 mm and 60 mm, as expanding the distance longer than 60 mm would required a larger computational domain, hence causing unnecessary increase in computational cost and time. Figure 2.17 illustrates the discharge coefficient from implementation of the aforementioned strategy, using different distances between orifice center to trough bottom. The left graph (a) represents the simulation using inlet flow of 0.388 kg/s whereas the right graph (b) covers the simulation results for 0.63 kg/s inlet flow rate.

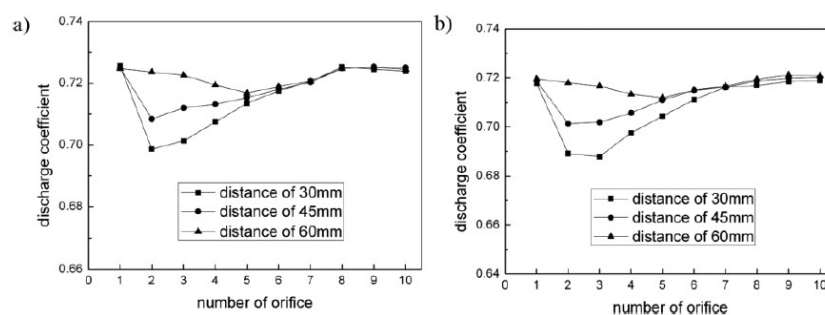


Figure 2.17: Comparison of Results with Different Distances (Yu, et al., 2013).

Based on the strategy results, Yu, et al. (2013) concluded that the impact of the strategy implemented is mostly on the orifices in high lateral velocity region such as orifices 2, 3 and 4. The reason behind the reduction in the effect of lateral velocity is because it separates the orifice from the high lateral velocity region. Therefore, as distance between the orifice center and bottom trough increases, it improves the uniformity of the orifice outflow in orifices 2 to 4 as shown in Figure 2.17.

2.2.7 Free and Submerged Flow of an Orifice Extended with Circular Pipe

Isenmann, et al. (2016) proposed the application of CFD to determine the discharge relationship in an pipe overflow structure, which often used as a circular broad-crested weir in urban drainage system, as shown in Figure 2.18. Regression analysis is implemented together with the data from CFD simulation

so to obtain an orifice equation, similar to the objective of the present project. Similar to the previous journals, VOF method is used to solve two-phase problem and $k-\omega$ Shear Stress Transport (SST) turbulence model was selected for the CFD simulation. To conclude, the orifice equation proposed by Isenmann, et al. (2016) is valid under the range of dimensions tested and are available for practical engineering applications.

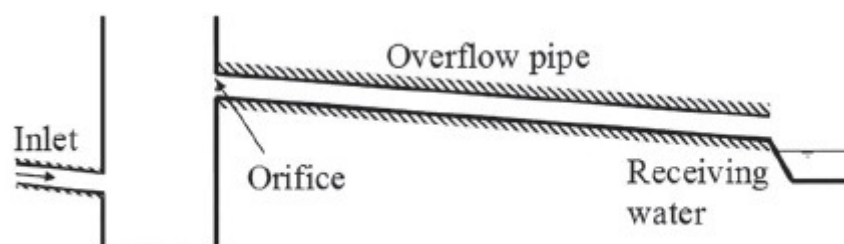


Figure 2.18: Schematic Diagram for Pipe Overflow Structure (Isenmann, et al., 2016).

2.2.8 Mutual Effect of Flow in Weir and Gate System

Sarhan and Jalil (2018) utilised the commercial software of FLOW-3D to simulate the combined system of weir and gate flow as shown in Figure 2.19. Due to having two types of flow, the discharge equations were determined to be both Rehbock formula and sluice gate's discharge equation, which are Eq.(2.6) and Eq.(2.3). In this literature, RNG $k-\epsilon$ turbulence model was deemed to be suitable to simulate the combined weir and gate flow that consists of chaos and unstable motion generated by eddies of various sizes. Gravitational acceleration in vertical direction was enabled with the setup of non-slip wall shear boundary. Pressure velocity coupling solvers were used to predict the simulation flow. Proceeding with the simulation results from Sarhan and Jalil (2018), the simulated discharge flow over weir in the combined system exhibits a flow behaviour that deviates from the traditional flow through sharp weir. In particular, the upstream flow behaves differently, so to satisfy the flow condition, leading to a higher discharge compared to the calculated one with decreases in percentage difference as the depth of flow, H increases. In fact, the weir in the combined system was found to have a better discharge performance, with 5 % to 20 % increases in discharge for the same head, h_1 if compared to

the traditional weir flow. The respective equations that correlate both weir discharge and gate discharge with the dimensionless parameters of H/d and h/d were formulated via IBM-SPSS 20 and listed as below,

$$Q_{weir} = 24.072 \left(\frac{h_1}{d} \right)^{0.535} - 4.416 \left(\frac{H}{d} \right)^{0.880} - 0.214, \quad R^2 = 0.958 \quad (2.10)$$

$$Q_{gate} = 5.475 \left(\frac{h_1}{d} \right)^{0.707} - 1225.168 \left(\frac{H}{d} \right)^{0.014} + 1261.689, \quad R^2 = 0.918 \quad (2.11)$$

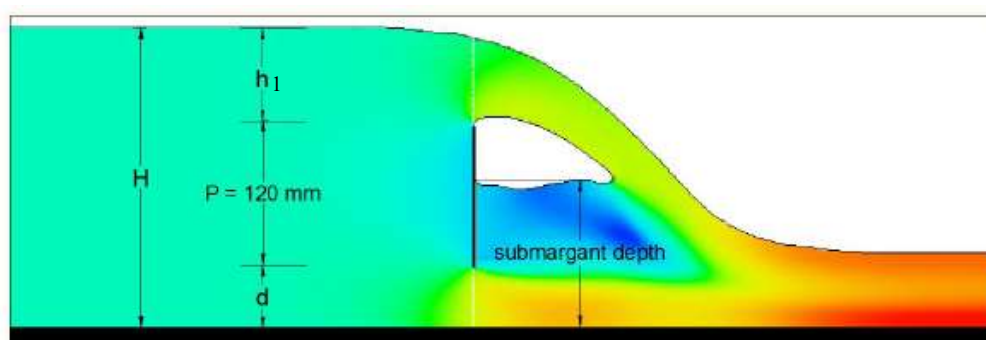


Figure 2.19: Schematic Diagram of the Combined System from Flow-3D (Sarhan and Jalil, 2018).

2.2.9 Free Flow through Side Rectangular Orifice

Hussain and Haroon (2019) published a research paper regarding the simulation of a free-surface flow through rectangular side orifice for numerical investigation under changing orifice width, L and sill height, W as shown in Figure 2.3. Three sets of orifice width value are used in the experiment including 4.4 cm, 8.9 cm and 13.3 cm whereas for the values used for crest height are the multiple of 5 from minimum value of 5 cm until the maximum value of 20 cm. In this simulation, the Finite Volume Method (FVM) is selected to solve the governing equations via ANSYS CFX as CFD solver. The reason for the selection of FVM rather than finite elements or finite differences is due to the suitability of the method itself for free-surface flows. The sketch for the computational fluid dynamic problems are shown in Figure 2.20.

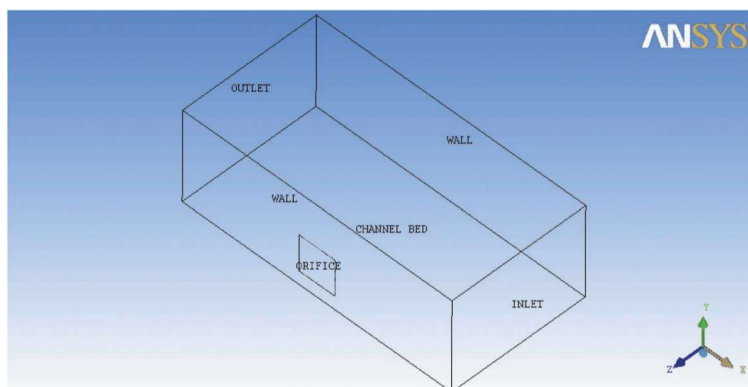


Figure 2.20: Computational Domain of Side Rectangular Orifice Model (Hussain and Haroon, 2019).

As illustrated in the figure above, respective boundaries are assigned and set to be coherent with the physical model. The following assumption was made while setting up the model's boundary condition:

- i) Velocity only flows in one direction of longitudinal at the inlet.
- ii) 'No slip' condition for 'WALL' boundary condition, at which the tangential fluid velocity is zero at solid boundary.
- iii) Bottom channel consist frictional effect due to roughness properties in the boundary.
- iv) Fluid assumed incompressible and monophasic.
- v) Negligible surface tension. ($Re > 1$, $Weber > 1$)

Meshing process of the domain is very important to produce an accurate result, whereby a non-proper meshing would contribute to divergence of numerical solutions, causing the variables to oscillate and cannot achieve converged solution. The meshing properties for the surrounding of side orifice was selected to be fine meshing whereas for rest of the domain, are chosen to be coarse. This is to provide more emphasis on the flow pattern at the orifice vicinity. The viscous model for this simulation was chosen to be k-epsilon model, allowing for the calculation of turbulence kinetic energy, k and dissipation rate, ϵ through two transport equations. This standard k-epsilon model is a two-equation turbulence model that assumes negligible molecular viscosity and full turbulence regime in the derivation of the model (Ansys, 2013). The model is comprised of scalable wall-function approach, which produces solutions with improved robustness and accuracy for finer meshes that are

located near wall. Furthermore, the model shown good agreement with experimental values for hydraulic problems with full turbulence flow. Tetrahedral meshing was employed as observed in Figure 2.21.

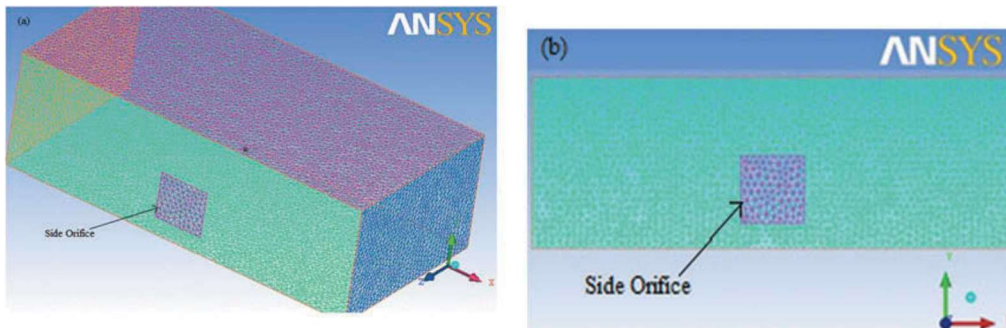


Figure 2.21: Tetrahedral Meshing (Hussain and Haroon, 2019).

The results of the study is validated against experimental data and good agreement between both results are achieved. Simulated results illustrates higher values if compared to the observed results as shown in Figure 2.22.

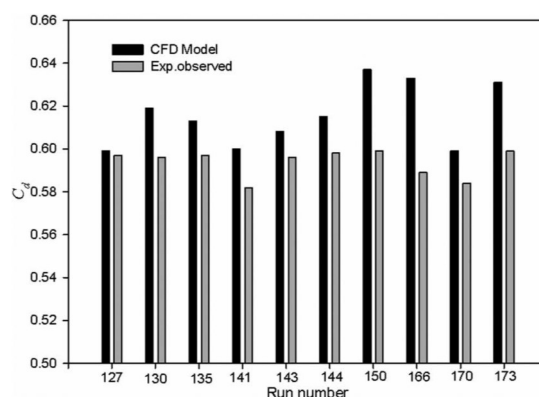


Figure 2.22: Comparison between Results in CFD Model and Experimental Model (Hussain and Haroon, 2019).

The reason behind the discrepancy of values was suspected to be caused by the setup in CFD model which neglects the flow viscous effect in side walls and channel bottom as well as the assumption of the approach velocity rather than using non-uniform velocity distribution (Hussain and Haroon, 2019). In general, this paper illustrate the capability and reliability of CFD simulations in helping to identify the flow behaviour and design side rectangular orifice for flow diversion purpose.

2.3 Summary

With respect to the problem statement in Chapter 1, Section 2.1 provides detailed introduction to the concerned events of **Case A, B and C**. **Case A** is essential in the present study as it serves to ascertain the suitability of the CFD simulation model. Nonetheless, Section 2.1.1 includes the literatures regarding free discharge flow through orifice as well as its associated models or equations, which is summarised under Table 2.5. The differences of using both circular orifice and rectangle orifice is also discussed under Section 2.1.1. On the other hand, Section 2.1.2 includes the reviews of past journals regarding partially submerged orifice. The literatures by Guo and Stitt (2017) and Brandes and Barlow (2012) provides promising guide on how the partially submerged orifice flow behaves. However, the models suggested by the aforementioned journals are not employed in this study, since their operating conditions does not correspond to that of the present study, which is free flow at both upstream and downstream. The application of pump is also involved in the above journals, whereby the water flow in the present study only depends on gravity and inertia.

Table 2.5: Summary of Models for Case A.

Operating Condition	Author	Model	Discharge Coefficient, C_d
Free discharge flow through gate/ rectangular orifice	(Bos, 1989; Ratnayaka, et al., 2009; Ojha and Subbaiah, 1997)	Eq.(2.3)	0.61
Free discharge flow through circular orifice	(Swamee and Swamee, 2010; Hussain, Ahmad and Asawa, 2010)	Eq.(2.4)	Table 2.1
Free discharge flow past through sluice gate	(Bos, 1989; Ratnayaka, et al., 2009; Kim, 2007)	Eq.(2.3)	Table 2.2

Free discharge flow through rectangular orifice (varying pressure head over flow area)	(Chadwick, et al., 2004; Doughlas et al., 2005)	Eq.(2.5)	0.61
Free flow past through weir	(Oshima, et al., 2013)	Eq.(2.6)	Eq.(2.7)

Section 2.2 relates to the CFD analysis and knowledge in simulating orifice flow or free surface problems by other authors. By having the same condition of open channel flow with the present study, these past researches can be useful in determining the simulation setup in terms of boundary condition, phase model, solution method, turbulence model, etc. Table 2.6 summaries the turbulence models implemented for the simulations included in this chapter.

Table 2.6: Viscous Models for CFD Simulations in Chapter 2.

Author	Simulation	Viscous Model
Chen, et al. (2002)	Turbulent overflow on stepped spillways	Standard $k-\varepsilon$ model
Kim (2007)	Free flow past a sluice gate	RNG $k-\varepsilon$ model
Mangarulkar (2010)	Side weir flow in open channel	RNG $k-\varepsilon$ model
Aydin (2012)	Free surface flow over triangular labyrinth side weir	RSM model
Mahmodinia, et al. (2012)	Free surface flow over side weir	RSM model
Yu, et al., (2013)	Orifice flow in a trough-type liquid distributor	SST $k-\omega$ model
Isenmann, et al. (2016)	Free and submerged flow of an orifice extended with circular pipe	SST $k-\omega$ model
Sarhan and Jalil (2018)	Mutual effect of flow in weir and gate system	RNG $k-\varepsilon$ model
Hussain and Haroon (2019)	Free flow through side rectangular orifice	Standard $k-\varepsilon$ model

CHAPTER 3

METHODOLOGY

3.1 Introduction

This chapter presents the governing equations, solver algorithm and methodology used for CFD ANSYS Fluent simulation of partially submerged circular orifice. The following sections present the theory of CFD, estimated parameters as well as the detailed approach on how to setup and run the CFD model.

3.2 CFD Theory

Navier-Stokes equations is the fundamental equation of all CFD equations, which describes the motions and forces that act on the model. They are governed as the equation of motion for a fluid and they represents the momentum conservation equations, stated in Eq.(3.1).

$$\frac{\partial}{\partial t}(\rho \vec{v}) + \nabla \cdot (\rho \vec{v} \vec{v}) = -\nabla p + \nabla \cdot \left[\mu \left[(\nabla \vec{v} + \nabla \vec{v}^T) - \frac{2}{3} \nabla \cdot \vec{v} I \right] \right] + \rho \vec{g} + \vec{F} \quad (3.1)$$

where ρ is the fluid density, t is time, \vec{v} is the fluid velocity vector, p represents the static pressure, μ is the molecular viscosity and I is the unit tensor. The left hand side of the equation corresponds to the inertia force while the right hand side of the equation represents the pressure, viscous, gravitational and external body force (Ansys, 2013).

Conservation of mass is governed by the continuity equation is written in Eq.(3.2).

$$\frac{\partial \rho}{\partial t} + \nabla \cdot (\rho \vec{v}) = S_m \quad (3.2)$$

Eq.(3.2) is the general form equation that accounts for mass conservation in both incompressible and compressible flows. Source S_m represents the external mass

added into the system from dispersed second phase as well as any other external sources (Ansys, 2013).

3.3 Orifice Geometry and Design

The CFD geometry model can be sketched and build by using the ANSYS Design Modeler incorporated in ANSYS Workbench. In this study, two models with similar dimensions were created, whereby the base model was simulated in 2-D and the final model was simulated in 3-D. The only difference between the 2-D and 3-D models is the orifice geometry, at which the base model has an opening with width spread across the model and the 3-D model has a typical sharp-edged circular orifice. As discussed previously, the 2-D base model was developed for verification of simulation whereas the 3-D model was a complete model that used to simulate **Case A**, **B**, and **C**. The dimension for both models was designed in the need to fit the parameters provided by industrial partner as shown in Table 3.1.

Table 3.1: Parameters for CFD Goemetry Model.

Parameters	Values
Orifice gap/diameter, d	Min: 15 mm; Max: 40 mm
Difference in water levels, Δh	≤ 100 mm (Case C : could be as small as 1 mm)
Thickness of the orifice wall, l	≤ 5 mm (e.g. a steel plate)
Depth of the vessel	Upstream: Few meters (≥ 1 m) Downstream: ≤ 500 mm

3.3.1 Base Model

The base model consist of an orifice with a thickness of 5 mm attached to two blocks of the same dimension (300 mm depth \times 100 mm width \times 150 mm long). In the base model, the width of the orifice is expanded throughout the model, representing infinite width and behaves similar to a gate as illustrated in Figure 3.1. This is to create a uniform flow across the width of the orifice, so that the results from the 2-D simulation would become the same regardless of which plane the translational symmetry is carried out to convert the model into a 2-D

model as shown in Figure 3.2. The dimensions for the base model in 2-D is illustrated in Figure 3.3.

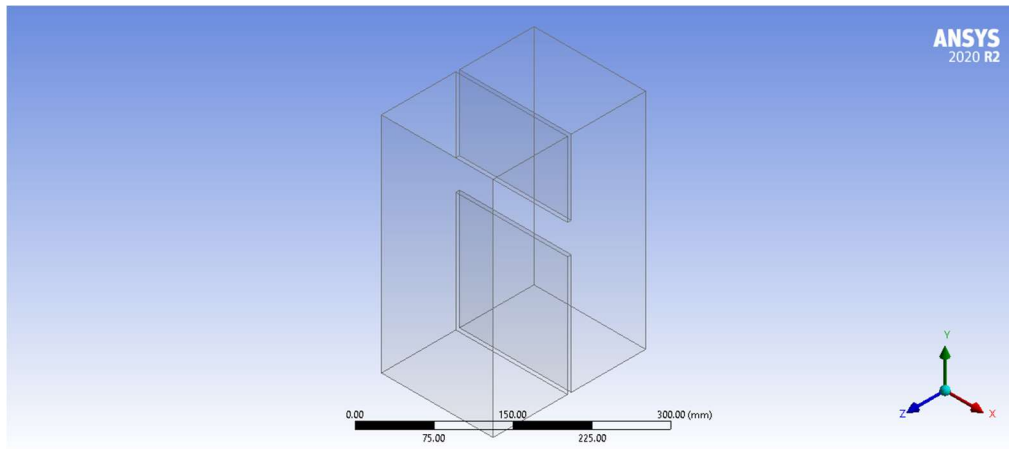


Figure 3.1: 3-D Sketch of Base Model.

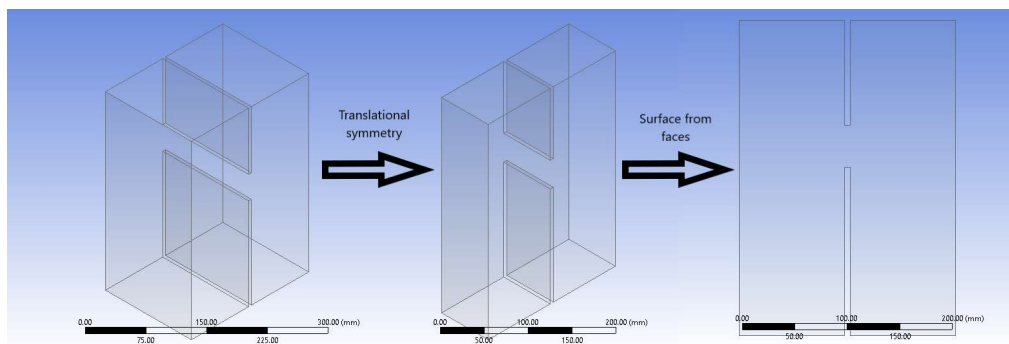


Figure 3.2: Translational Symmetry to Convert Base Model into 2-D.

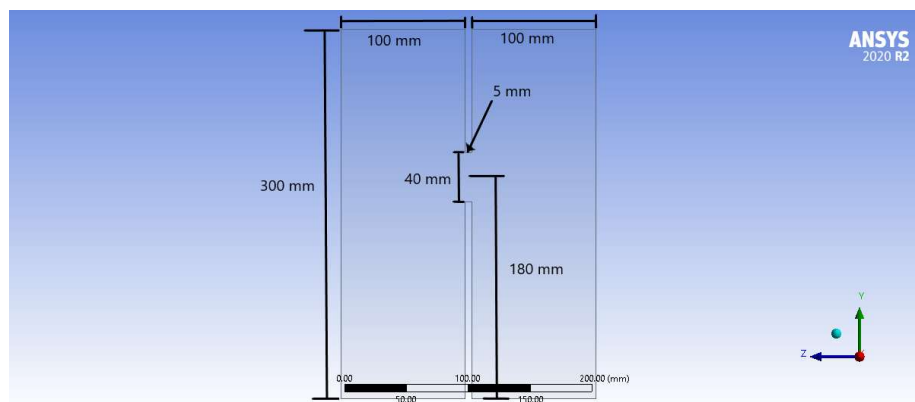


Figure 3.3: Dimensions for Base Model.

3.3.2 3-D Model

The geometry for the 3-D model is identical with the base model, at which it has an orifice with thickness of 5 mm attached to two blocks of same dimension (300 mm depth \times 100 mm width \times 150 mm long). The only difference is it consists of a circular orifice with the respective orifice parameters as shown in Table 3.1. Figure 3.4 depicts the geometry sketch for the 3-D model.

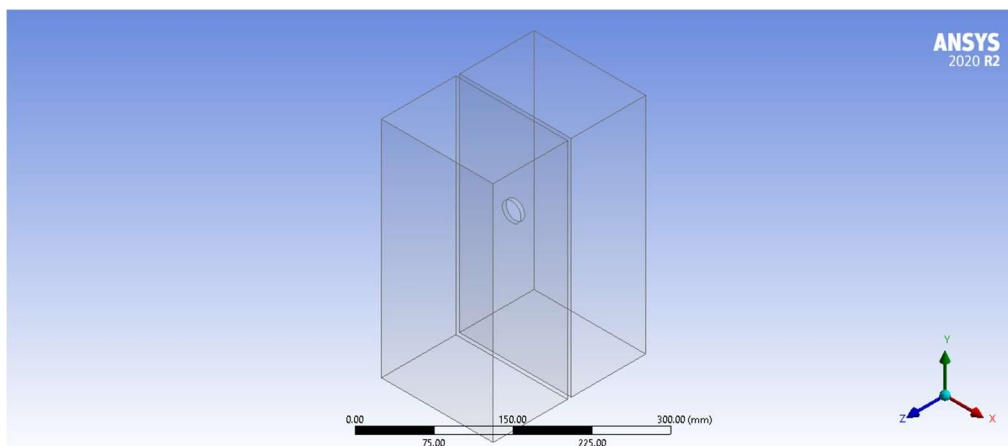


Figure 3.4: Sketch of the 3-D model.

3.4 Meshing

ANSYS Meshing application incorporated in ANSYS Workbench was used to setup the mesh of the model. The model was setup and generated by adapting the meshing properties from other researcher's work in Section 2.3 to the current study. The physics and solver preference under main meshing settings are selected to be CFD and Fluent, respectively. Referencing the meshing setup by Hussain and Haroon (2019) as well as Yu, et al. (2013), the meshing properties at the vicinity of the orifice was set to be finer compared to the rest of the domain as shown in Figure 3.5 and Figure 3.6, in which the element size for the cells around orifice are set to be 10 times smaller than the other domain cells. The reason is to provide a better resolution of the orifice flow, since higher quantity of cells meshing implies that all geometric details can be well captured, hence ensures that accurate simulation results are produced and the oscillating nature of the solution variables are prevented.

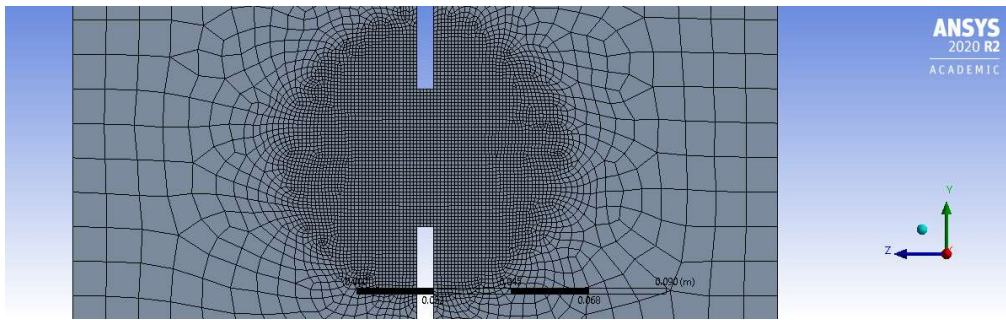


Figure 3.5: Finer Mesh Size around Orifice for Base Model.

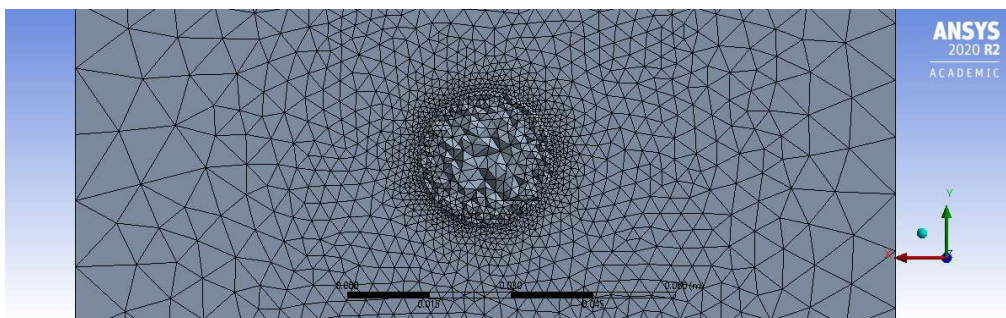


Figure 3.6: Finer Mesh Size around Orifice for 3-D Model.

Furthermore, the details for the mesh quality are checked under the quality criteria for the Mesh Metric. Quality check parameters such as skewness and orthogonal quality are applied to make the mesh uniform. For excellent mesh quality, the values of the skewness are recommended to be higher than 0.1 whereas the orthogonal quality have to be greater than 0.95 as shown in Figure 3.7.

Skewness mesh metrics spectrum					
Excellent	Very good	Good	Acceptable	Bad	Unacceptable
0-0.25	0.25-0.50	0.50-0.80	0.80-0.94	0.95-0.97	0.98-1.00

Orthogonal Quality mesh metrics spectrum					
Unacceptable	Bad	Acceptable	Good	Very good	Excellent
0-0.001	0.001-0.14	0.15-0.20	0.20-0.69	0.70-0.95	0.95-1.00

Figure 3.7: Mesh Quality Check Parameters (Ansys, 2015).

To ensure the mesh independence of the simulated solutions, mesh independence study was carried out. The purpose of this mesh independence test is to provide results with high confidence level. General concept of mesh

independence study is to continuously increase mesh size by reducing the global element size, and compares the results for each increase. For mesh independence analysis in this study, both models are tested via free discharge orifice flow (**Case A**) with upstream free surface water level set as 260 mm and bottom level set as -2000 mm to simulate the water depth of the upstream to be few metres deep according to Table 3.1. The orifice opening for base model is 40 mm whereas for 3-D model, the orifice diameter tested is 25 mm.

The initial element sizes for both models were 10 mm and 120 mm, respectively. By that, mesh quantity of the model was gradually increased by decreasing the global mesh size by 2 mm and 20 mm for base and 3-D model, respectively. The mesh size around the orifice was decreased tenfold compared to the domain element size and the percentage difference of the volumetric flow rate obtained with the volumetric flow rate from previous solution were recorded. The solution was defined mesh independent once the previous result display minimal difference of 0.1 % against the current result. Upon achieving the mesh independence, the smallest mesh resolution that contributes to the mesh independent solution are chosen to be the final solution.

3.5 Simulation Setup

Under the General setup in ANSYS Fluent, the pressure-based solver is selected to analyse the steady-state orifice fluid flow. As mentioned previously, the phenomenon is gravity driven as well as inertia dominated, therefore the gravitational acceleration is set to -9.81 m/s^2 at the y-direction. The fluids associated in this study is comprised of air and water only, at which their respective properties are set and copied from the Fluent Database. Referencing to the work by Chen, et al. (2002), Kim (2007), Mangarulkar (2010), Aydin (2012), Mahmodinia, et al. (2012), Aydin and Emiroglu (2013), Yu, et al. (2013) and Isenmann, et al. (2016) that involve simulations of multiphase flow, volume-of-fluid (VOF) method is selected as the multiphase model due to its well performance in tracing air and water. Under the VOF settings, open-channel flow is enabled. After a few attempts by trial and error, the solution method that was chosen to perform the simulation calculation was the Coupled scheme, since it provides the most stable solution if compared to PISO or Semi-Implicit Method for Pressure Linked Equations (SIMPLE) scheme. Furthermore,

Green-Gauss Node Based was chosen as the gradient option under the Spatial Discretization section because the method was found to be suitable for tetrahedral meshes. Based on Ansys (2013), the accuracy of node-based gradient in irregular unstructured meshes is greater when compared with the cell-based gradient.

Based on the literature review in chapter 2, various turbulence models are included in the researcher's CFD simulation for free surface flow as shown in Table 2.5. Therefore, by referencing the work of Aydin and Emiroglu (2013), the sensitivity of these turbulence models can be determined and compared based on their performance and computational time in simulation. Since free surface operating condition is involved in this study, the convergence in residuals as well as the parameters of interest were selected as the criteria to determine the best competent turbulence model, in which the number of iterations and computational time to reach convergence as well as the stability of the volumetric flow rate plot were compared. After several attempts, SST $k-\omega$ turbulence model was selected for both base model and 3-D model.

For both base model and 3-D model, the boundary conditions required to run the simulations are identical. The specifications for boundary conditions are set according to Figure 3.8 and Figure 3.9 for base model and 3-D model, respectively. Volumetric flow rate at the orifice center, as highlighted in Figure 3.10 was recorded, plotted and set as the output parameter. No slip velocity condition are assumed at the walls of the model. The top faces of the model are an entailment opening at atmospheric pressure and is set as pressure outlet with zero gauge pressure. Inlet and outlet of the model is set as pressure-inlet and pressure-outlet, respectively, with open-channel enabled. The open-channel function allows the user to determine the water depth of the upstream and downstream, by inserting y -values for the free surface level as well as the bottom level as shown in Figure 3.11 with the global coordinate system located as illustrated in Figure 3.12. Bottom level for the inlet and outlet is set as -2000 mm and 0 mm, respectively, so to simulate their depth in the practical condition as shown in Table 3.1 while the free surface level is manipulated according to the water flow event.

After setting the boundary conditions and initialization, the regions where the initial water level lies would be marked using the adapt function under

the domain tab. Patch feature is then implemented to simulate the initial water level by setting the water volume fraction of the region as 1. For 3-D model, mesh adaption feature is utilised with volume of fluid as predefined criteria, so as to reduce the fluctuation nature in multiphase model. This feature allows ANSYS Fluent to refine and coarsen the mesh based on the initial water level set, at which the mesh at the water surface level is refined and the rest of the domain are coarsen.

In this study, the convergence criteria for the simulation was judged on the residuals plot, volumetric flow rate plot, and the water volume fraction contour. To achieve a better convergence in this multiphase problem, “**solve/set/multiphase-numeric/default-controls/recommend-default-for-existing-cases/yes**” and “**solve/set/multiphase-numeric/stable-vof-settings/yes/2**” are key in to the console window. Both of these commands allow ANSYS Fluent to conduct changes in the controls and settings for the simulation, so to achieve better and stable converged solution. Under relaxation factor (URF) is adjusted manually if the solution becomes unstable and was not able to converge. The plot for volumetric flow rate is ensured to be constant as it reaches the end of the simulation until the solution is converged. If the fluctuations in volumetric flow rate persist, it indicates the presence of unsteady flow, and the simulation would resolve to a transient solver instead of a steady solver. Monitor residuals is set to 0.001 for steady solver and 0.0001 for transient solver according to Mahmodinia, et al. (2012). On the other hand, the contour for water volume fraction is observed throughout the calculation, so to ensure that the flow behaviour is close or similar to the practical event.

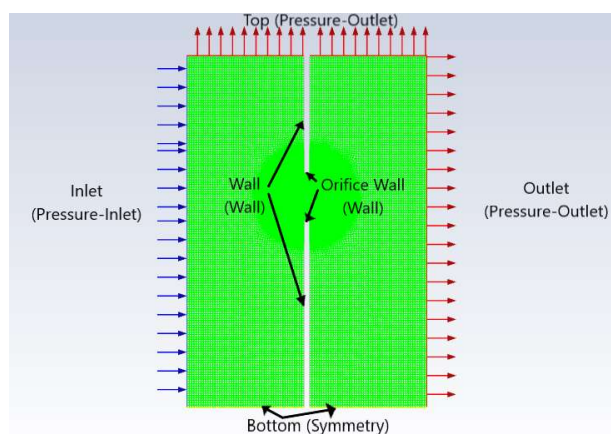


Figure 3.8: Boundary Conditions for Base Model.

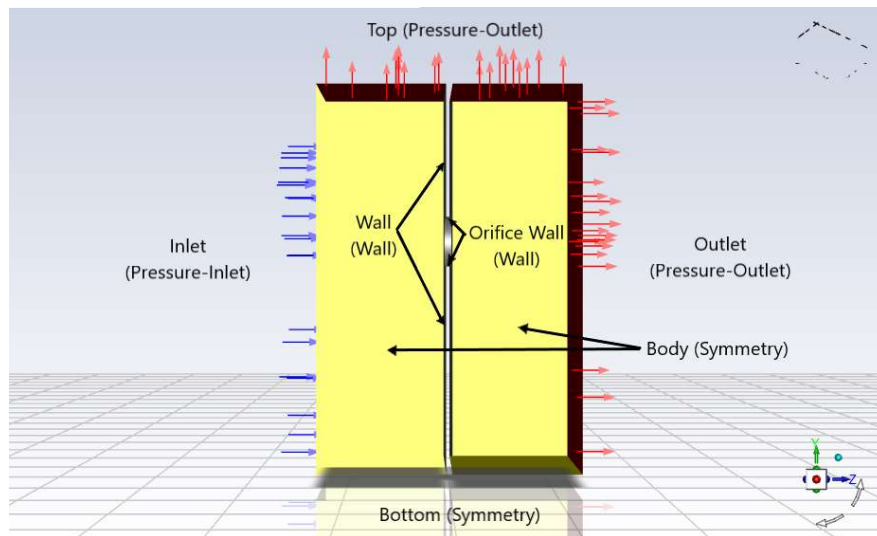


Figure 3.9: Boundary Conditions for 3-D model.

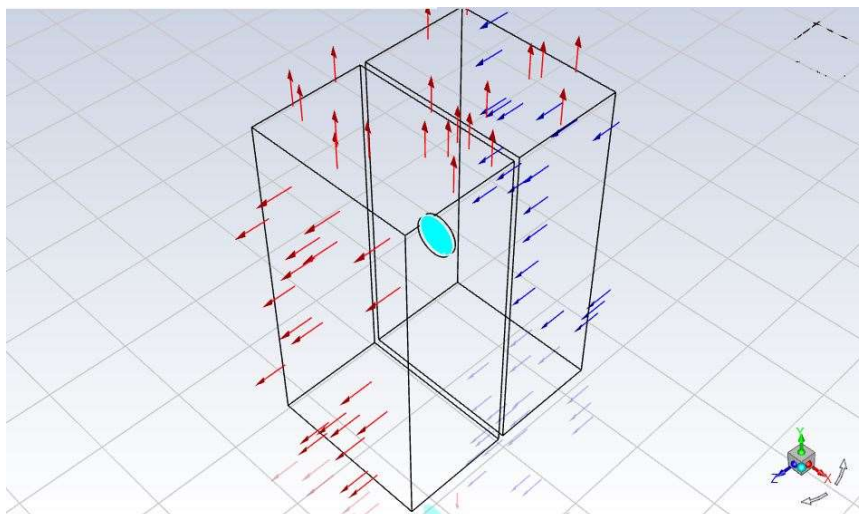


Figure 3.10: Surface where Volumetric Flow Rate is Measured.

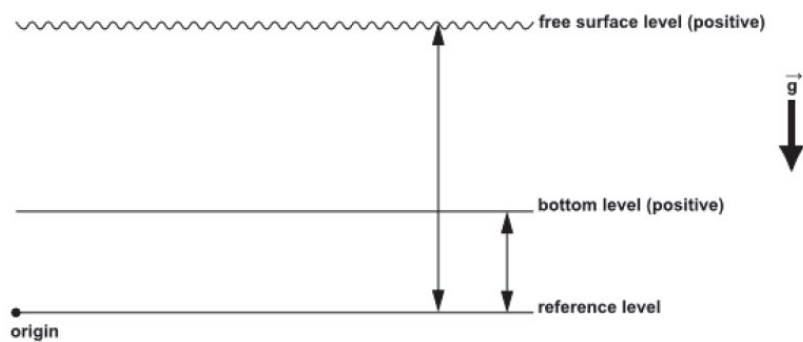


Figure 3.11: Free Surface Level and Bottom Level (Ansys, 2013).

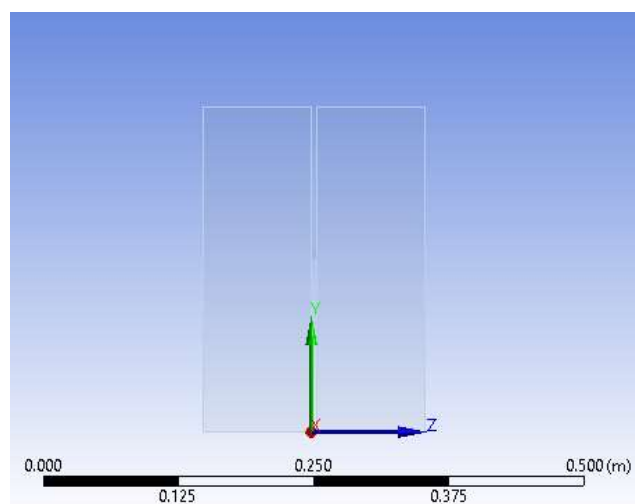


Figure 3.12: Location for Global Coordinate System.

By using the simulation setup above, the CFD simulations for **Case A**, **B** and **C** were carried out. For **Case A**, the outlet for both models is set as zero gauge pressure, so to simulate atmospheric condition whereas the inlet was set to different water surface level depending on the flow event. The base model was validated by simulating a free discharge flow through water gate and free flow through a sharp-crested weir with gate opening of 40 mm. The former results were compared with the calculated values using the classic orifice discharge equation (Eq.(2.3)) and the discharge coefficient was assumed to be 0.61 according to Bos (1989) and Ratnayaka, et al. (2009). The upstream water surface level were simulated from 290 mm and decrease by 10 mm for each simulation. On the other hand, the results from simulating weir flow were verified against the Rehbock formula (Eq.(2.6)) and the upstream water surface level were simulated from 165 mm to 195 mm. Since base model is a 2-D model, at which the width of the orifice is removed through translational symmetry, the parameter of interest for base model would be the volumetric flow rate per meter width, i.e. the width of orifice or gate is assumed to be 1 m.

The validation of 3-D model was carried out using free discharge flow through circular orifice (Eq.(2.4)). The discharge coefficient for the equations was retrieved from Table 2.1, as tabulated from the research by Bos (1989). Since the range of orifice diameter used in this study is listed in Table 3.1, only orifice diameter of 20 mm, 25 mm and 35 mm were included in the validation

of 3-D model. The upstream water surface level were simulated from 220 mm to 280 mm for each orifice size.

For **Case B**, the water surface level at the downstream domain, h_2 was set as 180 mm whereas the upstream water surface level was manipulated between 220 mm to 280 mm, so as to observe the effect of water level difference, Δh on the volumetric flow rate, Q . Effects of different orifice diameter, d is also simulated from 15 mm to 40 mm according to Table 3.1. On the other hand, the water level on both sides was manipulated for **Case C**, so that it was not higher or lower than the orifice opening. Similar to the simulations for **Case B**, the orifice diameter, d is simulated from 15 mm to 40 mm according to Table 3.1.

Visual analysis of the orifice flow, at which the velocity and volume fraction distribution shown in the simulated contour diagrams were compared and evaluated. To ascertain the suitability of CFD software, the output parameters of volumetric flow rate at orifice center were recorded and compared with the calculated volumetric flow rate from Eq.(2.3) and Eq.(2.6) for base model and Eq.(2.4) for 3-D model. After completing the validation of model, the simulation for **Case B** and **C** using the 3-D model were executed and the results were plotted in graphs. By referring to Sarhan and Jalil (2018), the correlations of the tested variables were also formulated as regression equations via IBM SPSS using the simulated results. Considering the practicality of this study, the values for volumetric flow rate was recorded in unit of cubic meter per hour (m^3/h) with 2 decimal places for the results and discussion section.

CHAPTER 4

RESULTS AND DISCUSSION

4.1 Mesh Independence Analysis

The mesh independence test was performed for base model and 3-D model by monitoring the percentage difference between the simulated results of different mesh sizes. The results are tabulated in Table 4.1 and the mesh independent solution was determined when the percentage difference is lower than 0.1 %. By that, the smallest mesh resolution that contributes to the mesh independent solution are chosen to be the final solution.

The mesh independence analysis concludes that the solution with 9786 element cells was the mesh independent solution for base model whereas the solution with 90905 element cells was the final solution for 3-D model. The former consists of element mesh size of 8 mm while the latter is meshed with cell size of 100 mm. On the other hand, the mesh size at the vicinity of orifice for the aforementioned solutions were 0.8 mm and 10 mm, respectively.

Table 4.1: Mesh Independence Analysis for Both Models.

Model	Number of Cells	Volumetric Flow Rate, (m ³ /h)	Percentage Difference (%)
Base model	6527	117.04	-
	9786	114.78	1.9
	16689	114.89	0.1
	36166	114.35	0.5
	139017	113.99	0.3
3-D model	89988	1.33	-
	90905	1.33	0.5
	94501	1.34	0.1
	105732	1.34	0.1
	145862	1.34	0.2
	201854	1.34	0.2

4.2 Case A – Free Discharge Flow through Orifice

Before the main simulation in this study was executed, both base and 3-D model are required to be verified using free flow through orifice (**Case A**), since this case is extensively studied over the past few decades and the research regarding this phenomenon is abundant.

4.2.1 Base Model

Table 4.2 illustrate the verification results of free discharging condition for base model. Based on Table 4.2, it can observed that the percentage difference increases as the water depth decreased. This is due to the decrease in hydrostatic pressure as the water level decreases, at which the amount of pressure forcing the water to enter the orifice decreases. This could also be explained by the increase in the width of the vena-contracta as the water level decreases, indicating a decreases in the amount or degree of jet contraction, as shown in Figure 4.1. Furthermore, it can also be noticed that water surface level lowered than 0.23 m was not included in the simulation for free discharge flow in base model. This is because the the volume fraction contour of the simulation display the presence of air entering the orifice, hence indicating incomplete submergence of orifice opening in the upstream. That is to say, even though the water surface level was set higher than the orifice gate, but the flow simulated would be similar to a weir flow due the absence of water flowing into the orifice from sideways since it is constructed as a 2-D model. However, the overall results show good agreement with the model from Bos (1989) and Ratnayaka, et al. (2009), with percentage difference of 2.6 % to 6.6 %.

On the other hand, Table 4.3 represent the deviation of the results from weir flow simulation against Rehbock formula with the base model. The outcome of simulating weir flow with base model yields 2.8 % to 38.1 % deviation from the Rehbock model. According to Table 4.3, it is clear that the deviation with the Rehbock formula increases as the water surface level increases. To be exact, the volumetric flow rate obtained from the simulation tends to overshoot from the Rehbock formula given by Oshima, et al. (2013). The reason suspected for the discrepancies in volumetric flow rates was due to the low weir head, h_l . In this study, the water flow is driven by gravity and inertia, so the required momentum to discharge the weir flow to atmospheric

solely depends on the weir head, h_1 . Since the orifice opening was set to a maximum value of 40 mm according (Table 3.1), the weir head, h_1 for the weir flow of base model cannot exceed 0.04 m, at which the water surface level must be lower than 0.20 m. However, for such low values of weir head, h_1 , the water flow would not be discharged to the air but travels downwards along the wall as shown in Figure 4.2. Nonetheless, the validation of base model using models from Bos (1989), Ratnayaka, et al. (2009) and Oshima, et al. (2013) achieved reasonable agreement in terms of trendline and values.

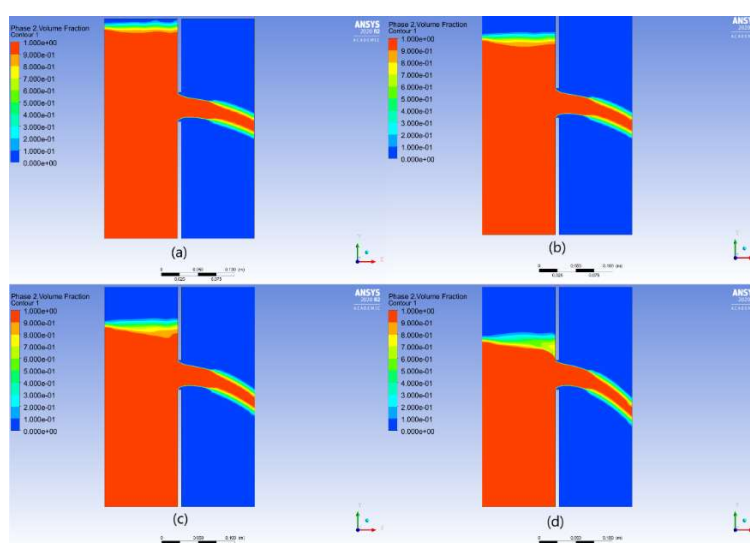


Figure 4.1: Volume Fraction Contour of Free Discharge Flow through Water Gate at Different Water Surface Level. Red Colour Indicates Water and Blue Colour Indicates Air. (a) 290 mm, (b) 270 mm, (c) 250 mm and (d) 230 mm.

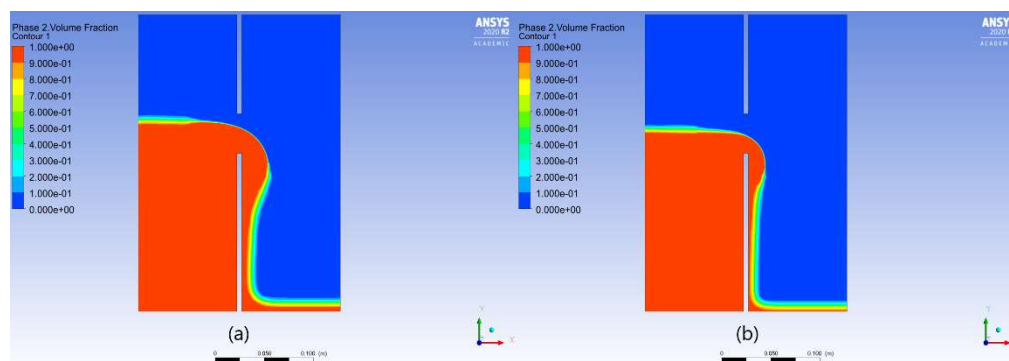


Figure 4.2: Volume Fraction Contour of Free Discharge Flow through Weir at Different Water Surface Level. Red Colour Indicates Water and Blue Colour Indicates Air. (a) 195 mm and (b) 185 mm.

Table 4.2: Validation of Base Model with Free Discharge Flow through Water Gate.

Water Surface Level (mm)	Volumetric Flow Rate from CFD, Q_{CFD} (m³/h)	Calculated Volumetric Flow Rate, Q (m³/h) using Eq.(2.3)	Percentage difference (%)
290	132.43	129.04	2.6
280	126.77	123.04	3.0
270	120.76	116.72	3.5
260	114.35	110.05	3.9
250	107.50	102.94	4.4
240	100.61	95.31	5.6
230	92.70	87.00	6.6

Table 4.3: Validation of Base Model with Weir Flow.

Water Surface Level (mm)	Volumetric Flow Rate from CFD, Q_{CFD} (m³/h)	Calculated Volumetric Flow Rate, Q (m³/h) using Eq.(2.6)	Percentage difference (%)
195	56.34	45.30	24.4
190	45.04	36.08	24.8
185	35.74	27.62	29.4
180	24.80	19.99	24.0
175	15.49	13.27	16.7
170	7.35	7.57	2.8
165	1.90	3.07	38.1

4.2.2 3-D Model

Table 4.4 illustrates the verification results of free discharge flow through circular orifice with Eq.(2.4). The overall results for 3-D model illustrates good agreement with the models from Bos (1989), with only 0.4 % to 8.7 % deviation. Unlike the validation of free discharge flow in base model, all orifices are fully submerged in the upstream due to high volume of fluid and the presence of water

entering the circular orifice from sideways in the 3-D model as shown in Figure 4.3 and Figure 4.4. Furthermore, Table 4.4 depicts that the developed model show strong agreement in term of trend with the Bos (1989) model, whereby the volumetric flow rate increases as the water surface level and orifice diameter increased.

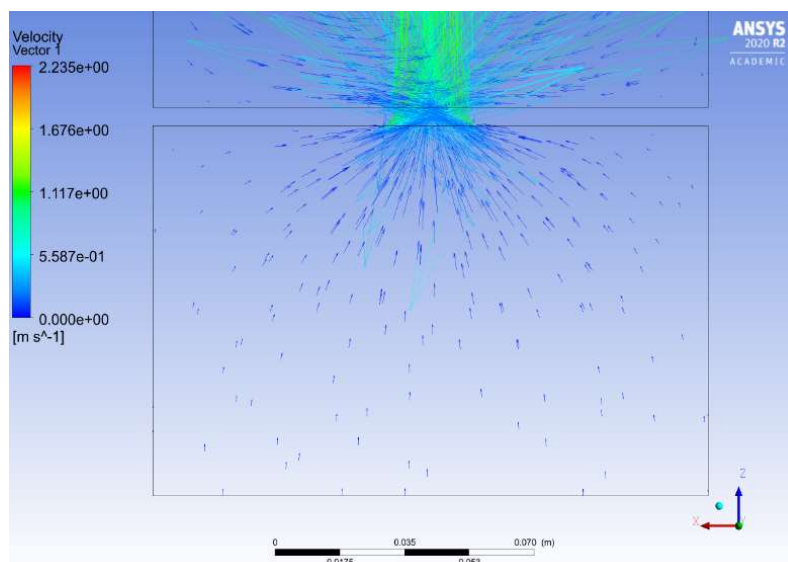


Figure 4.3: Velocity Vectors at the Upstream Domain Case A (Top View).

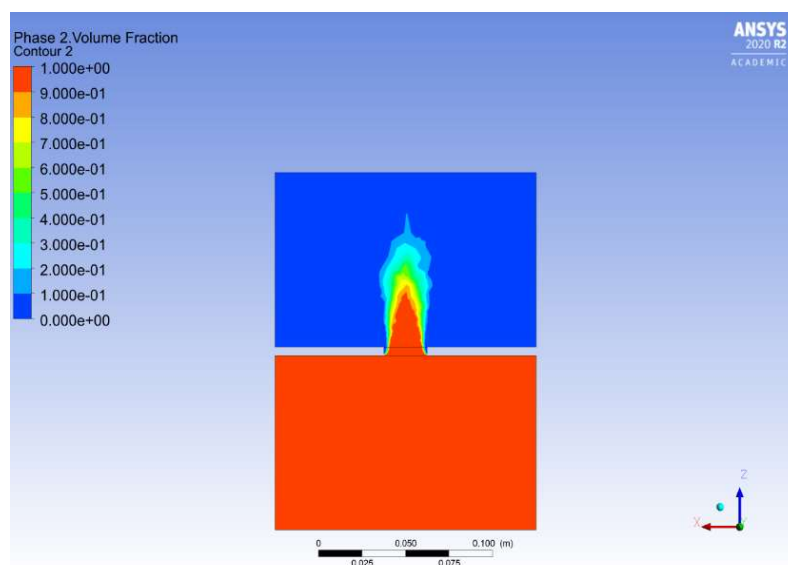


Figure 4.4: Volume Fraction Contour at the Upstream Domain Case A (Top View). Red Colour Indicates Water and Blue Colour Indicates Air.

Table 4.4: Validation of 3-D model Free Discharge Flow through Circular Orifice.

Orifice Diameter, d (mm)	Water Surface Level (mm)	Volumetric Flow Rate from CFD, Q_{CFD} (m ³ /h)	Calculated Volumetric Flow Rate, Q (m ³ /h) using Eq.(2.4)	Percentage difference (%)
20	280	0.96	0.96	0.4
	260	0.87	0.86	0.5
	240	0.76	0.75	2.1
	220	0.64	0.61	4.5
25	280	1.50	1.53	2.6
	260	1.34	1.37	2.6
	240	1.16	1.19	2.1
	220	0.98	0.97	1.0
35	280	2.83	3.10	8.7
	260	2.59	2.78	6.7
	240	2.27	2.41	5.5
	220	1.84	1.96	6.1

In general, the outcomes from simulating **Case A** with 3-D model provides promising agreement with the models from Bos (1989), hence provide confidence that the model developed is applicable for the subsequent simulations for the partially submerged circular orifice flow (**Case B** and **Case C**).

4.3 Case B – Partially Submerged at Orifice Outlet

Using the 3-D model, the conditions of water flowing through partially submerged orifice at the downstream (**Case B**) is simulated. The flow behaviour for **Case B** was demonstrated in Figure 4.5 and Figure 4.6, whereby the water from the inlet enters the orifice, causing an increase in water level near the outlet side of the orifice, but gradually decreases as it approaches the outlet boundary layer. As indicated by the colour change from red to light blue in Figure 4.5 and Figure 4.6, the water volume fraction decreased from high to low, showing a

decrease in water level. By that, the flow behaviour shows good agreement with the real condition, since the outlet portion of the liquid is continuously drained away due to the presence of free surface flow in the outlet domain.

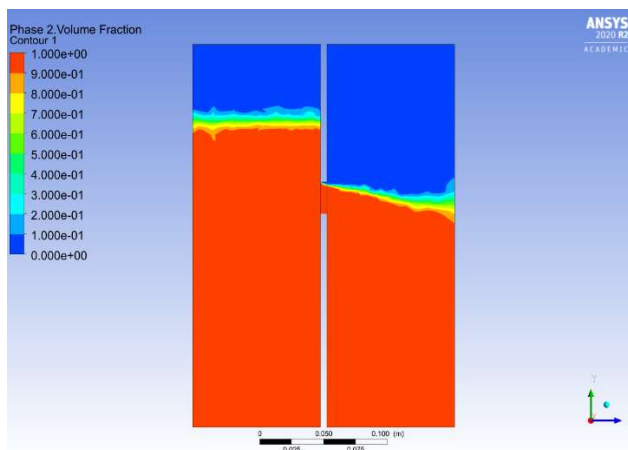


Figure 4.5: Volume Fraction Contour at the Upstream Domain Case B (Side View). Red Colour Indicates Water and Blue Colour Indicates Air.

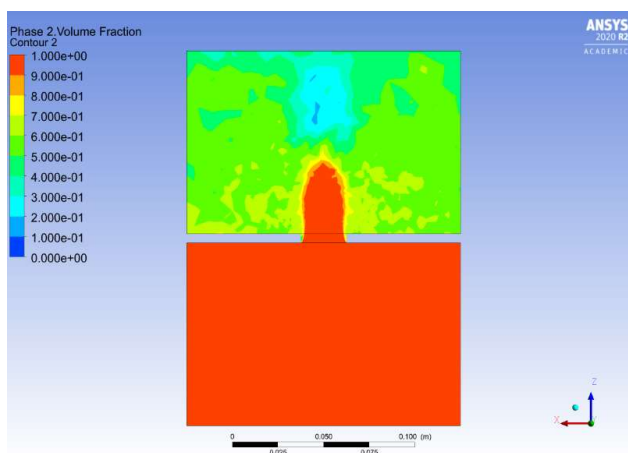


Figure 4.6: Volume Fraction Contour at the Upstream Domain Case B (Top View). Red Colour Indicates Water and Blue Colour Indicates Air.

Figure 4.7 illustrates the graph of volumetric flow rate, Q against water level difference, Δh at different orifice diameter, d for **Case B**. According to Figure 4.7, a visible trend was observed, whereby the volumetric flow rate, Q increases as the water level difference, Δh and orifice diameter, d increased. It can also be observed that the changes in volumetric flow rate is significantly smaller if the orifice size is small. Therefore, it can be deduced that the effect of orifice diameter, d is more significant than that of the water level difference, Δh

on the volumetric flow rate, Q . This is because larger orifice diameter allows higher volume of fluid to pass through, even though the water level difference is the same. Moreover, if compared to the free discharge flow through orifice, the volumetric flow rate is slightly lower. The reason might be due to the presence of water level at the outlet, causing the differential in pressure between inlet and outlet to decrease. Therefore, the water particles that passes through the orifice have a lower velocity, leading to a decrease in volumetric flow rate. The decrease in velocity of water travelling through the orifice is shown in Figure 4.8, in which the velocity vectors are observed with the aid of the legend attached.

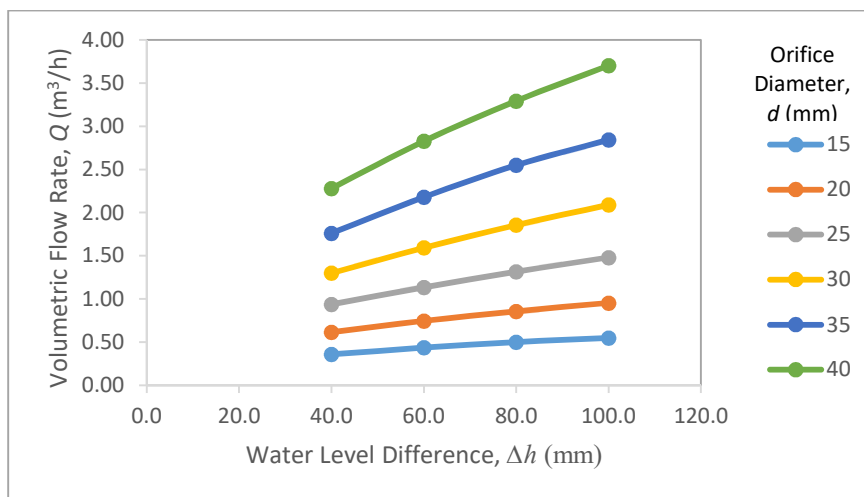


Figure 4.7: Volumetric Flow Rate, Q against Water Level Difference, Δh at different Orifice Diameter, d (Case B).

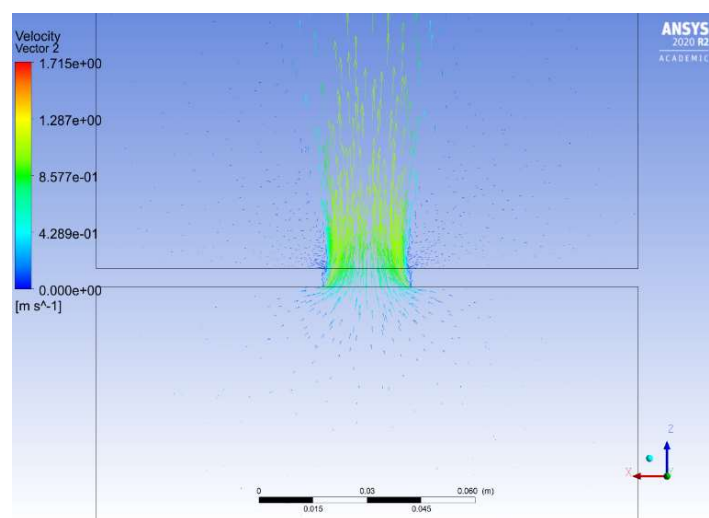


Figure 4.8: Velocity Vectors at the Upstream Domain Case B (Top View).

Referencing the study by Sarhan and Jalil (2018), IBM SPSS Statistics 25 is employed for the correlation study of **Case B**. To correlate the orifice discharge with the geometrical dimensionless parameters of $\Delta h/h_2$ and d/h_2 , where h_2 is the downstream water surface level, the statistical nonlinear regression analysis is executed using the IBM SPSS software. The regression equation that represents the correlation of the model developed for **Case B** is,

$$Q = 2.5824 \left(\frac{\Delta h}{h_2} \right)^{0.5318} + 60.2747 \left(\frac{d}{h_2} \right)^{1.9987} - 1.4977, \quad R^2 = 0.971 \quad (4.1)$$

4.4 Case C – Partially Submerged at Both Inlet and Outlet

The operating condition for **Case C** is almost identical to **Case B**, in which it is partially submerged condition but with both sides of the orifice partially submerged. The flow behaviour for **Case C** is demonstrated in Figure 4.9 and Figure 4.10, whereby the water flows from inlet to the outlet that has a lower water surface level. Based on Figure 4.9, it can be seen that the flow behaves more similar to a flow through circular weir, in which the upstream domain overflow to the downstream due to difference in water surface level. The orifice discharge distance was also noticed to be shorter in Figure 4.10 due to low hydrostatic pressure at the upstream domain, leading to a lower discharge velocity and volumetric flow rate as shown in Figure 4.11.

The results obtained from simulating the flow past through partially submerged circular orifice of **Case C** is illustrated in Figure 4.12, in which it displays the relationship of orifice discharge with the water level difference and orifice dimension. Based on Figure 4.12, the same trend from **Case B** is observed for **Case C**, where volumetric flow rate, Q increases as the water level difference, Δh and orifice diameter, d increased. Furthermore, the effect of orifice diameter, d tends to be more significant than that of the water level difference, Δh on the volumetric flow rate, Q . The same reason is also applied for **Case C**, in which larger orifice diameter allows higher volume of water to pass through. However, the trend is not significant if the water level difference is too small as shown in Figure 4.12. This is because of the difference in

hydrostatic pressure between upstream and downstream is too small, causing the volumetric flow rates to be similar even though the orifice size is different.

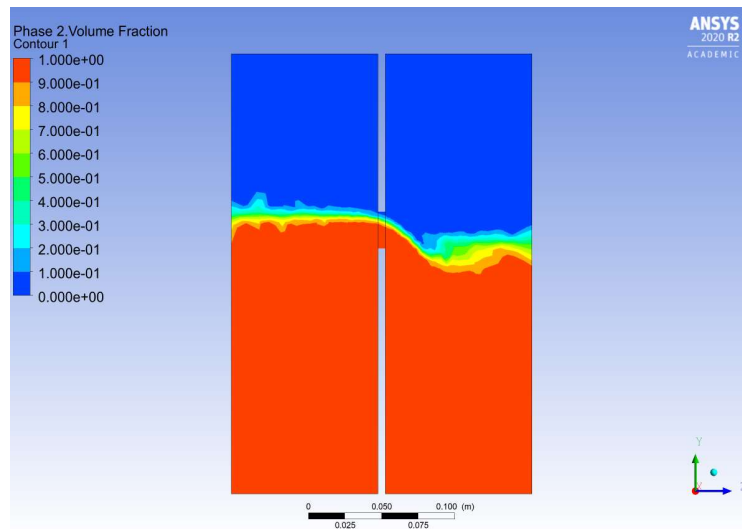


Figure 4.9: Volume Fraction Contour at the Upstream Domain Case C (Side View). Red Colour Indicates Water and Blue Colour Indicates Air.

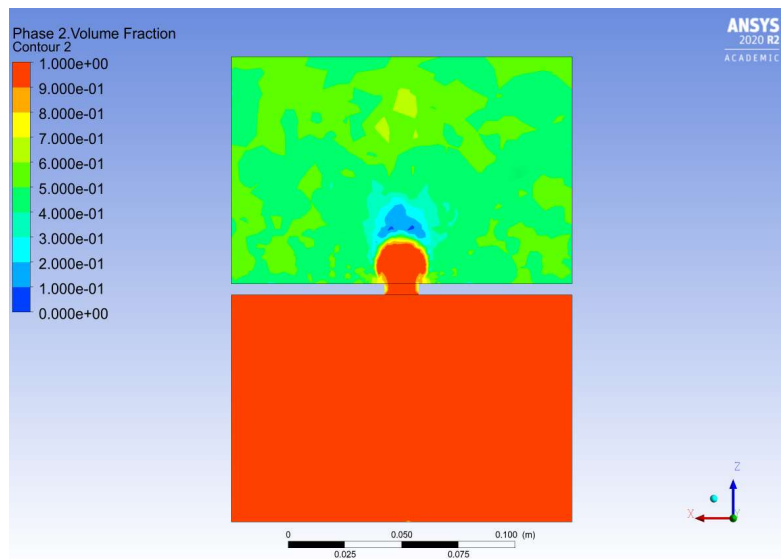


Figure 4.10: Volume Fraction Contour at the Upstream Domain Case C (Top View). Red Colour Indicates Water and Blue Colour Indicates Air.

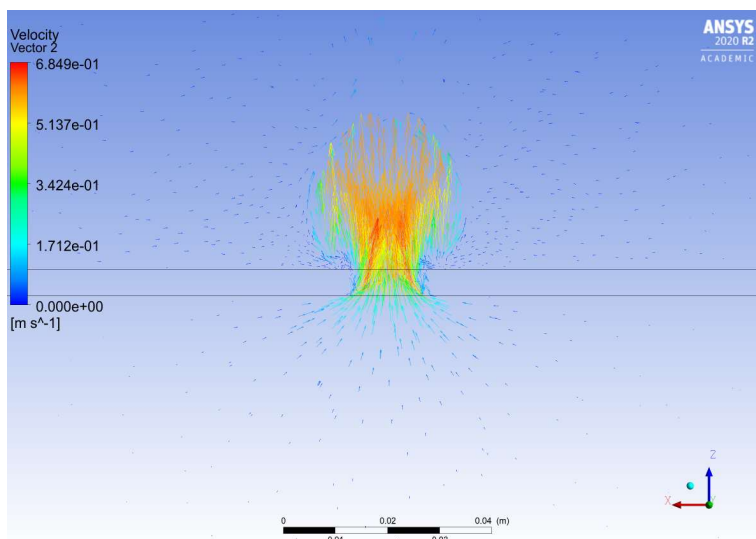


Figure 4.11: Velocity Vectors at the Upstream Domain Case C (Top View).

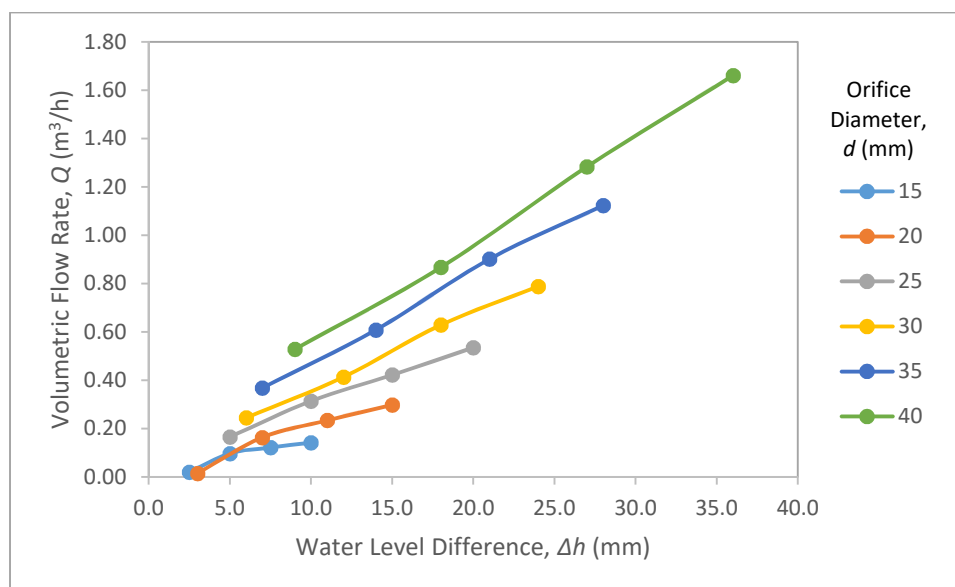


Figure 4.12: Volumetric Flow Rate, Q against Water Level Difference, Δh at different Orifice Diameter, d (Case C).

The same procedure as in **Case B** was carried out to correlate the volumetric flow rate, Q with the geometrical dimensionless parameters of $\Delta h/h_2$ and d/h_2 in **Case C**. A mathematical model is produced using the non linear regression analysis in IBM SPSS Statistics 25. The outcome of the analysis is listed as below,

$$Q = 11.1256 \left(\frac{\Delta h}{h_2} \right)^{1.4498} + 13.1821 \left(\frac{d}{h_2} \right)^{2.3960} - 0.0479, \quad R^2 = 0.994 \quad (4.2)$$

CHAPTER 5

CONCLUSION AND RECOMMENDATIONS

5.1 Conclusion

As a conclusion, **Case A, B and C** were successfully simulated using ANSYS Fluent and the results were evaluated and analysed. Within the study limitations, this project leads to the following findings:

1. The CFD models developed display promising agreement with the models from Ratnayaka, et al. (2009), Oshima, et al. (2013) and Bos (1989), having discrepancies in the range of 0.4 % to 38.1 %.
2. The hypothesis that volumetric flow rate increases as the water level difference and orifice diameter increase in partial submerged condition was proven for **Case B and C**.
3. The effect of orifice diameter on the volumetric flow rate is greater than that of the water level difference.
4. Correlation for volumetric flow rate with water level difference and orifice diameter for **Case B and C** were obtained through the CFD simulation and were represented by Eq.(4.1) and Eq.(4.2), respectively.

5.2 Recommendations

Even though CFD simulation is a powerful tool that provides accurate predictions, its application has its limitation, where it may slightly deviates from the real situation due to simplified boundary conditions. Despite knowing that the scope of this study is limited, improvements could be made through the following suggestions.

Flow 3D is suggested as the CFD software. ANSYS Fluent is sufficient to obtain accurate results for the free surface problems in this study, but the results can be improved by Flow 3D. This is because the equation for mass and momentum in Flow 3D is based on VOF method and the software consists of air entrainment feature that benefits in capturing the rate at which gas is entrained into the flow. This feature can provide better insights of the flow behaviour, especially at the outlet, where air entrainment may occur due to the orifice discharge and turbulence in the liquid.

REFERENCES

- Adam, N.J., Cesare, G.D.E. and Schleiss, A.J., 2017. Head Losses and Influence Length of Sharp-Edged and Rounded Orifices Under Steady Flow Conditions. 1(1), pp.3045–3050.
- Ansys, I., 2009. ANSYS CFX-Solver Theory Guide. 15317(April), pp.724–746.
- Ansys, I., 2013. ANSYS Fluent Theory Guide. *ANSYS Inc., USA*, [online] 15317(November), pp.724–746. Available at: <http://www.afs.enea.it/project/neptunius/docs/fluent/html/th/main_pre.htm>.
- Aydin, M.C., 2012. CFD simulation of free-surface flow over triangular labyrinth side weir. *Advances in Engineering Software*, [online] 45(1), pp.159–166. Available at: <<http://dx.doi.org/10.1016/j.advengsoft.2011.09.006>>.
- Aydin, M.C. and Emiroglu, M.E., 2013. Determination of capacity of labyrinth side weir by CFD. *Flow Measurement and Instrumentation*, [online] 29, pp.1–8. Available at: <<http://dx.doi.org/10.1016/j.flowmeasinst.2012.09.008>>.
- Barlow, W.T. and Brandes, D., 2015. Stage-discharge models for concrete orifices: Impact on estimating detention basin drawdown time. *Journal of Irrigation and Drainage Engineering*, 141(12), pp.1–7.
- Borghei, S.M., Jalili, M.R. and Ghodsian, M., 1999. Discharge Coefficient for Sharp-Crested Side Weir in Subcritical Flow. *Journal of Hydraulic Engineering*, 125(10), pp.1051–1056.
- Bos, M.G., 1989. *Discharge measurement structures*. 3rd Revised ed. Wageningen, The Netherlands: Publication 20. International Institute for Land Reclamation and Improvement, Wageningen, The Netherlands.
- Brandes, D. and Barlow, W.T., 2012. New Method for Modeling Thin-Walled Orifice Flow under Partially Submerged Conditions. *Journal of Irrigation and Drainage Engineering*, 138(10), pp.924–928.
- Chadwick, A., Morfett, J. and Borthwick, M., 2004. *Hydraulics of Civil and Environmental Engineering*. 4th ed. New York: Spon Press.
- Chen, Q., Dai, G. and Liu, H., 2002. Volume of fluid model for turbulence numerical simulation of stepped spillway overflow. *Journal of Hydraulic Engineering*, 128(7), pp.683–688.
- Datawave Marine Solutions, 2019. *PRACTICAL CFD MODELING: Judging Convergence* - YouTube. [online] Available at: <https://www.youtube.com/watch?v=hti4gDuSoRs&ab_channel=DatawaveMarineSolutions> [Accessed 9 Apr. 2021].

Doughlas, J.F., Gasoriek, J.M., Swaffield, J. and Jack, L., 2005. *Fluid Mechanics*. 5th ed. New York: Prentice Hall.

Eghbalzadeh, A., Javan, M., Hayati, M. and Amini, A., 2016. Discharge prediction of circular and rectangular side orifices using artificial neural networks. *KSCE Journal of Civil Engineering*, 20(2), pp.990–996.

Emin Emiroglu, M., Kisi, O. and Bilhan, O., 2010. Predicting discharge capacity of triangular labyrinth side weir located on a straight channel by using an adaptive neuro-fuzzy technique. *Advances in Engineering Software*, [online] 41(2), pp.154–160. Available at: <<http://dx.doi.org/10.1016/j.advengsoft.2009.09.006>>.

Ghodsian, M., 2003. Flow through side sluice gate. *Journal of Irrigation and Drainage Engineering*, 129(6), pp.458–463.

Guo, J.C.Y. and Stitt, R.P., 2017. Flow through partially submerged orifice. *Journal of Irrigation and Drainage Engineering*, 143(8), pp.2–4.

Guo, J.C.Y. and Urbonas, B., 1996. Maximized detention volume determined by runoff capture ratio. *Journal of Water Resources Planning and Management*, 122(1), pp.33–39.

Hussain, A., Ahmad, Z. and Asawa, G.L., 2010. Discharge characteristics of sharp-crested circular side orifices in open channels. *Flow Measurement and Instrumentation*, [online] 21(3), pp.418–424. Available at: <<http://dx.doi.org/10.1016/j.flowmeasinst.2010.06.005>>.

Hussain, A., Ahmad, Z. and Asawa, G.L., 2011. Flow through sharp-crested rectangular side orifices under free flow condition in open channels. *Agricultural Water Management*, [online] 98(10), pp.1536–1544. Available at: <<http://dx.doi.org/10.1016/j.agwat.2011.05.004>>.

Hussain, A., Ahmad, Z. and Ojha, C.S.P., 2014. Analysis of flow through lateral rectangular orifices in open channels. *Flow Measurement and Instrumentation*, [online] 36, pp.32–35. Available at: <<http://dx.doi.org/10.1016/j.flowmeasinst.2014.02.002>>.

Hussain, A. and Haroon, A., 2019. Numerical analysis for free flow through side rectangular orifice in an open channel. *ISH Journal of Hydraulic Engineering*, [online] 00(00), pp.1–8. Available at: <<https://doi.org/10.1080/09715010.2019.1648220>>.

Isenmann, G., Bellahcen, S., Vazquez, J., Dufresne, M., Joannis, C. and Mose, R., 2016. Stage–discharge relationship for a pipe overflow structure in both free and submerged flow. *Engineering Applications of Computational Fluid Mechanics*, [online] 10(1), pp.283–295. Available at: <<https://doi.org/10.1080/19942060.2016.1157100>>.

Karki, B., 2018. *chapter 7 flow measurements*. [online] Available at: <<https://www.slideshare.net/BinuKarki/080118-chapter-7-flow-measurements>> [Accessed 12 Sep. 2020].

Kim, D.-G., 2007. Numerical analysis of free flow past a sluice gate. *KSCE Journal of Civil Engineering*, 11(2), pp.127–132.

Kubrak, M., 2015. Assessment of equivalence of small and large orifice computational models. *Archives of Hydroengineering and Environmental Mechanics*, 63(3–4), pp.67–76.

Mahmodinia, S., Javan, M. and Eghbalzadeha, A., 2012. The effects of the upstream Froude number on the free surface flow over the side weirs. *Procedia Engineering*, 28(2011), pp.644–647.

Mangarulkar, K., 2010. Experimental and numerical study of the characteristics of side weir flows. (November).

Nago, H., 1978. Influence of gate-shapes on discharge coefficients. *Trans. Japanese Soc Civil Engr*, [online] 10, pp.116–119. Available at: <https://www.jstage.jst.go.jp/article/jscej1969/1978/270/1978_270_59/_article/-char/ja/> [Accessed 20 Jan. 2021].

Ojha, C.S.P. and Subbaiah, D., 1997. Analysis of flow through lateral slot. *Journal of Irrigation and Drainage Engineering*, 123(5), pp.402–405.

Oshima, M., Ishido, T. and Boiten, W., 2013. Discharge Coefficient for Full-Width Sharp-Crested High Weirs. *Journal of JSCE*, 1(1), pp.360–365.

Peritus, 2019. *The Benefits and Limitations of Computational Fluid Dynamics in the Offshore Oil and Gas Industry - Peritus*. [online] Available at: <<https://www.peritusint.com/benefits-and-limitations-of-computational-fluid-dynamics/>> [Accessed 20 Aug. 2020].

Pretechnologies, 2020. *Advantages of CFD | FEA services and consultancy. CFD and FEA company*. [online] Available at: <<http://www.pretechnologies.com/services/computational-fluid-dynamics/advantage>> [Accessed 20 Aug. 2020].

Rajaratnam, N. and Subramanya, K., 1967. Flow Equation for the Sluice Gate. *J.Irrigation and Drainage Eng., ASCE*, 93(3), pp.167–186.

Ramamurthy, A.S., Tim, U.S. and Rao, M.V.J., 1987. Weir-orifice units for uniform flow distribution. *Journal of Environmental Engineering (United States)*, 113(1), pp.155–166.

Ratnayaka, D.D., Brandt, M.J., Johnson, K.M., Ratnayaka, D.D., Brandt, M.J. and Johnson, K.M., 2009. CHAPTER 12 – Hydraulics. *Water Supply*, pp.463–498.

Roth, A. and Hager, W.H., 1999. Underflow of standard sluice gate. *Experiments in Fluids*, 27(4), pp.339–350.

Sarhan, S.A. and Jalil, S.A., 2018. Analysis of Simulation Outputs for the Mutual Effect of Flow in Weir and Gate System. *Journal of University of Babylon for Engineering Sciences*, 26(6), pp.48–59.

Singh, R., Manivannan, D. and Satyanarayana, T., 1994. Discharge coefficient of rectangular side weirs. *Journal of Irrigation and Drainage Engineering*, 120(4), pp.814–819.

Swamee, P.K., Pathak, S.K. and Ali, M.S., 1993. Analysis of rectangular side sluice gate. *Journal of Irrigation and Drainage Engineering*, 119(6), pp.1026–1035.

Swamee, P.K. and Swamee, N., 2010. Discharge equation of a circular sharp-crested orifice. *Journal of Hydraulic Research*, 48(1 EXTRA ISSUE), pp.106–107.

Taghvaeian, S., n.d. Irrigation Water Flow Measurement. *Division of Agricultural Sciences and Natural Resources. Oklahoma State University*, (2).

Thajudeen, A., 2018. *Orifices | Classification of Orifices | Hydraulic Co-efficient | CivilDigital* |. [online] Available at: <<https://civildigital.com/orifices-classification-of-orifices-hydraulic-co-efficient/>> [Accessed 23 Aug. 2020].

USBR Water Measuremen Manual, 2020. *Chapter 9 - SUBMERGED ORIFICES, Section 1. Definition and Classification of Orifices*. [online] Available at: <https://www.usbr.gov/tsc/techreferences/mands/wmm/chap09_01.html> [Accessed 14 Aug. 2020].

Yu, H., Li, X., Sui, H., Xu, C. and Li, H., 2013. Simulation of orifice flow influenced by lateral flow in a trough-type liquid distributor. *Chemical Engineering and Technology*, 36(11), pp.1975–1984.

APPENDICES

APPENDIX A: TABLE

Table A-1: Volumetric Flow Rate, Q at Different Water Level Difference, Δh and Orifice Diameter, d (Case B).

Orifice Diameter, d (mm)	Water Level Difference, Δh (mm)	Volumetric Flow Rate, Q (m ³ /h)
15	100.0	0.55
	80.0	0.50
	60.0	0.44
	40.0	0.36
20	100.0	0.95
	80.0	0.86
	60.0	0.75
	40.0	0.62
25	100.0	1.48
	80.0	1.32
	60.0	1.14
	40.0	0.94
30	100.0	2.09
	80.0	1.86
	60.0	1.59
	40.0	1.30
35	100.0	2.84
	80.0	2.55
	60.0	2.18
	40.0	1.76
40	100.0	3.70
	80.0	3.29
	60.0	2.83
	40.0	2.28

Table A-2: Volumetric Flow Rate, Q at Different Water Level Difference, Δh and Orifice Diameter, d (Case C).

Orifice Diameter, d (mm)	Water Surface Level at Downstream Domain, h_2 (mm)	Water Level Difference, Δh (mm)	Volumetric Flow Rate, Q (m³/h)
15	175	10.0	0.14
		7.5	0.12
		5.0	0.10
		2.5	0.02
20	172	15.0	0.30
		11.0	0.23
		7.0	0.16
		3.0	0.02
25	170	20.0	0.54
		15.0	0.42
		10.0	0.31
		5.0	0.17
30	167	24.0	0.79
		18.0	0.63
		12.0	0.41
		6.0	0.25
35	165	28.0	1.12
		21.0	0.90
		14.0	0.61
		7.0	0.37
40	162	36.0	1.66
		27.0	1.28
		18.0	0.87
		9.0	0.53